Supporting Information

Biomimetic catalysis of nitrite reductase enzyme using copper complexes in chemical and electrochemical reduction of nitrite

Millena P. Ferreira[a], Caio B. Castro[a], João Honorato [a,c], Sheng He [e], Charlene Esmieu[d], Eduardo E. Castellano[c], Daniela R. Truzzi[b], Otaciro R. Nascimento[c], Antoine Simonneau[d], Caterina G.C. Marques Netto[a,e]

a- *Rod. Washington Luiz, km 235 s/n, Departamento de Química, Universidade Federal de São Carlos (UFSCar) – São Carlos, Brazil*

b- *Departamento de Bioquímica, Instituto de Química de São Paulo, Universidade de São Paulo, Caixa Postal 26077, CEP05513-970 São Paulo, São Paulo, Brazil*

c- *Instituto de Física de São Carlos, Universidade de São Paulo (USP), Av. João Dagnone, 1100, Jardim Santa Angelina, São Carlos, São Paulo 13563-120, Brazil*

d- *LCC-CNRS, Université de Toulouse, CNRS, UPS, 205 route de Narbonne, BP44099, F-31077 Toulouse cedex 4, France*

e- *Department of Chemistry, Emory University, Atlanta, GA 30322*

*caterina@ufscar.br

Index

Methods

1.1- X-Ray diffraction

Ligand PTB (CCDC 2113820) and complex CuPTPh (CCDC 2113821) were crystallized in methanolic solutions by slow solvent evaporation. Data collection of the monocrystals were performed in a mini diffractometer Rigaku XtaLAB with MoKα radiation and graphite monochromate (λ = 0,71073 Å). Cell refinements, data reduction and integration were performed using CrysAlisPro software and the solution and refinement of the structures were obtained using SHELX, host on OLEX2 software. The multi-scan method was used to correct the absorption. Table representations ans structures were generated by OLEX2 and MERCURY, respectively..

1.2- FTIR

1.2.1 Solid state FTIR

Fourier Transform Infrared (FTIR) spectra were obatined in KBr pellets using a Bomen-Michelson FT spectrometer model MB-102. All measurements were onbtained in the interval of 400 and 4000 cm^{-1}.

1.2.2 Phototitration

FTIR spectra were recorded using a modified Varian 660 FT-IR spectrometer. For transmission FTIR, the IR beam is picked off through an external sample chamber to an

external detector. The sample is loaded into a sample cell consisting of a 75 μm PTFE spacer between two CaF_2 windows (Harrick) held in a copper housing. All transmission FTIR spectra are the average of 1200 scans. All spectra are ratioed to the spectrum of unphotolyzed *o*-NBA in methanol or CuPTP. Prior to any illumination, initial spectra are obtained. The sample is illuminated at 351 nm with a Nd:YLF laser (Crystalaser) for a set length. Following illumination, spectra are obtained, and the process is repeated. CuPTP was used in 35mM, o-NBA and sodium nitrite were used in 35mM final concentrations.

1.3 Electronic spectroscopy in the UV-Vis region

1.3.1 Molar absorptivity and copper reduction assays

Electronic spectra were recorded in a HP – Hewlett Packard 8452 A spectrophotometer. The samples were analyzed in solution using a quartz cell with 1mL maximum volume and optical path of 1.0 cm. values of molar absorptivity, ε, were calculated using the maximum absorbance value of the bands from the Lambert-Beer law ($\varepsilon = A/bC$), in which A = absorbance, b = optical path and C = concentration in mol L^{-1}.

1.3.2 Stepwise addition of reagents and Ligand binding constant

The stepwise addition of nitrite, ascorbate and acid was monitored via an Ocean Optics spectrometer. The reaction was stirred using a magnetic stir bar and spectra were recorded every 100ms. The reaction occurred at room temperature.

For the ligand binding constant experiment, a 1mM solution of CuPTB was titrated with aliquots of 1μL of 0.1M of the ligands and the reaction was monitored via an Ocean Optics spectrometer.

1.4- Electronic Paramagnetic Resonance (EPR)

Measurements were recorded at room temperature (296K) and at liquid nitrogen temperature (77K). For the measurements an EPR equipment model Varian E109, X band, using a rectangular cavity and modulation at 100 kHz. The parameters for the measurements were power of micro-wave (20mW), modulation amplitude (0.4mT peak to peak) with automatic gain for each sample, field scanning of 160mT, 0.064s. Scanning of 3 minutes. To calibrate

the magnetic field an EPR standard was emploed (MgO:Cr(III) g = 1.9797 crystal) and the ressonance frequency was measured with a micro-wave frequency meter.

1.5 – Microanalysis

All microanalyses were performed by the Analytical Central from the Department of Chemistry at UFSCar using an EAGER 200 CE equipment.

1.6 Conductivity measuments

All conductivity measurements were obtained from 1mM methanolic solutions in the conductivity meter Meter Lab model CDM230. The obtained values were compared from black solutions (solvent) and the standard electrolytic region.

1.7- Electrochemical measurements

The electrochemical measurements were performed using an EG&G potentiostat Princeton Applied Research Model 273A/ A conventional glass cell with three electrodes was used. The electrodes used were vitreous carbon (0,071 cm^2), platin and $Ag_{(s)}/AgCl_{(s)}|KCl^-$ (3.5M) as working, auxiliar and reference electrodes, respectively. All measurements were performed in methanol containing tetrabutylammonium perchlorate 0.1M as an electrolyte. To remove dissolved oxygen, argon was purged in the cell for 15 minutes prior to each scan. The working electrode was polished with alumina 0.05μm before the experiments, followed by washing with water. The auxiliar and reference electrodes were washed with methanol prior to their addition to the cell.

a. Determination of k_{cat} and K_M from electroreduction experiments

The graphic from Figure 9B (V_{NO} *vs* $[NO_2]$) was made by using the catalytic currents from Figure 9A, S37 and S38 in a similar way to literature. [1] The V_{NO} values were obtained by dividing the current density by the Faraday constant, resulting in a NO formation by electrode area unity (V_{NO}, nmol s^{-1} cm^{-2}). The value of k_{cat} was obtained dividing V_{max} by the catalyst concentration. Since the medium is not stirred, the catalyst concentration corresponds to the number of molecules that participate in the electrochemical reaction and can be determined by integrating the charge that is formed in the redox process (Cu(II)/Cu(I)) in the absence of substrate. Therefore, the integration indicates a concentration of electrochemically active surface of 2.5 x 10^{-10} mol. cm^{-2}.

1.8- Nuclear Magnetic Resonance (NMR)

All ^{1}H, ^{13}C, and 2D NMR spectra were obtained in a 400 MHz BRUKER ARX 9.4 T.

NMR spectra were obtained from solutions of deuterated chloroform ($CDCl_3$) or acetone $(CD_3)_2CO$ with residual solvent serving as an internal standard. NMR shifts were reported in parts per million (ppm). Abbreviations for signal multiplicity are as follow: s = singlet, d = doublet, t = triplet, q = quartet, m = multiplet, dd = doublet of doublet, etc. Coupling constants (J values) were calculated directly from the spectra. ^{15}N NMR were recorded in methanol-D_4 and referenced to liquid ammonia. The ^{15}N NMR were recorded in a 600 MHz in a Bruker 600 spectrometer.

1.9- Mass spectrometry

Ligands had their mass determined by methane chemical ionization and the complexes were ionized by electrospray (ESI).

1.10 Stopped-flow

Kinetics studies were performed in an upgraded Applied Photophysics model SX-18 MV stopped-flow spectrophotometer with either a photomultiplier tube (PMT) or a photodiode array (PDA) used as the detector. The stopped-flow analysis was performed at 10°C and all solutions were deaerated before the measurement. Two solutions were prepared: one containing sodium ascorbate (1mM) in methanol and the other containing (1mM of the copper complex), 50 eq. Of benzoic acid and the nitrite concentration was varied to achieve a final concentration of 1mM, 5mM, 10mM, 15mM and 20mM.

1.11 DFT calculations

The most challenging aspect of the computational modeling of metal complexes is the correct assignment of the conformations/configurations of the ligands. The crystallographic structures are provide an adequate starting point for the modeling, but we adopted several protocols to properly sample the structural diversity of the systems under investigation, as we hereafter describe. We performed an ensemble search for conformers of the complexes within 8.0 kJ/mol of the minimum energy conformer using the meta-dynamics package CREST[2] driven by the semi-empirical density functional tight binding theory with the GFN1-xTB Hamiltonian[3] as implemented into the xtb program[4] (version 6.6.0). Solvent effects were computed with the Generalized Born model augmented with the solvent accessible surface area to compute the hydrophobic interactions (GBSA [5]) using methanol as the solvent. The

lowest energy conformers were then subjected to full geometric optimization and vibrational frequencies calculation. Further conformational sampling was performed by means of ab initio molecular dynamics simulations carried out using xtb program and analyzed with VMD built-in tools. The equations of motion were integrated up to 50 ps with a timestep of 1 fs at the temperature of 298 K[6]. We also computed the electronic excitation spectra with simplified Tamm-Dancoff approach (sTDA [7]) as implemented in the stda program (version 1.6.1).

2. Ligand synthesis and characterization

The difference between the ligands were a radical moiety connected to the triazole, obtaining a phenyl (PTPh), *n*-butyl (PTB) and *n*-propanol (PTP) modified ligand. As shown in scheme 1, the synthesis started with the methylation of L-proline using $SOCl_2$ in methanolic solution, followed by the alkylation of the nitrogen using 2-chloromethyl pyridine, yielding 82% of compound (2). After a Grignard reaction with phenylmagnesium bromide, compound (3) was obtained in 42% yield. The reaction of compound (3) with sodium azide under acidic conditions resulted in the formation of (4), which was used in a click-reaction protocol to obtain ligands, as shown in scheme S1. The ligands were characterized by FTIR, HRMS, ^{1}H, ^{13}C NMR confirming their structures. Ligand PTB was also characterized by X-ray crystallography, as shown in Figure S42.

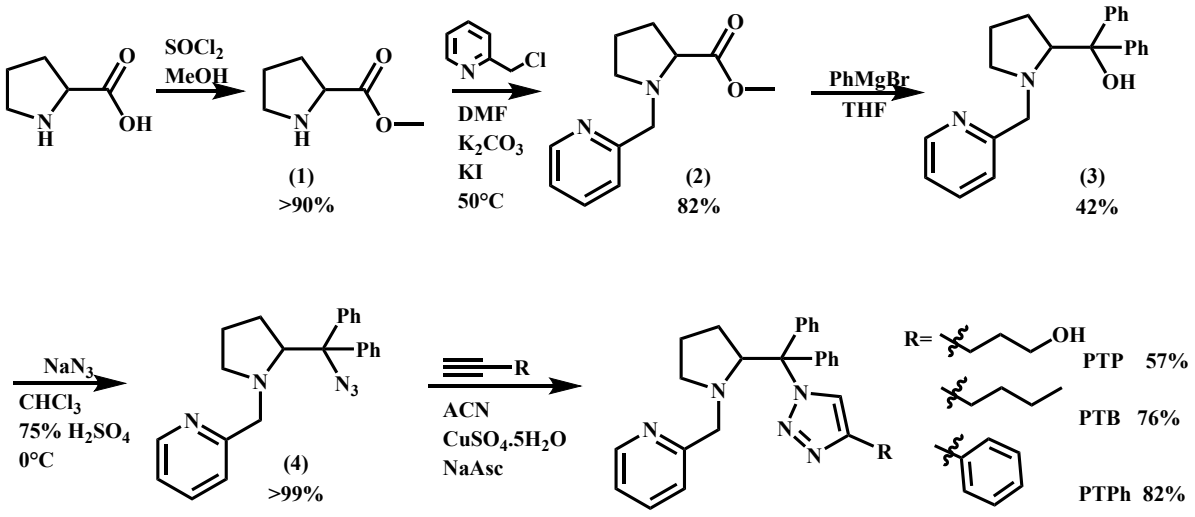

Scheme S1. Scheme of the synthesis of ligands PTPh, PTB e PTP.

Synthesis of methyl L-prolinate (1) and methyl (pyridin-2-yl-methyl) prolinate (2)

To a 250-mL Schlenk flask were added 40 mL of anhydrous methanol. The methanol was cooled to 0°C using an ice bath prior to the dropwise addition of 8.4 mL (0.115 mol) of $SOCl_2$. After that, 12 g of L-proline (0.104 mol) were added to the solution and the reaction was kept at room temperature for 24 hours. The solvent and excess $SOCl_2$ were removed by evaporation to obtain 13.2 g of a light-yellow oil. The whole content of this reaction was dissolved into 70 mL of DMF, followed by the addition of 33 g of Na_2CO_3 (0.311 mol), 18.8g (0.114 mol) of 2-(chloromethyl) pyridine hydrochloride and 7.91g of KI (0.047 mol). This mixture was kept under stirring at 50 °C for 16 hours. After that period, 50 mL of water were added, and the reaction content was extracted with dichloromethane (3 x 30 mL). The organic phase was dried with $MgSO_4$, filtered and the solvent was removed under reduced pressure to obtain a dark-red oily product in 82% yield.

^{1}H NMR: (400 MHz, $CDCl_3$): δ 8.54 (dd, J= 1.2 Hz, 1H); 7.65 (m, 1H); 7.47 (d, J=7.8 Hz, 1H); 7.17 (m, 1H); 4.06 (d, J= 13.5 Hz,1H); 3.80 (d, J= 13.5 Hz, 1H); 3.67 (s, 3H); 3.44 (m, 1H); 3.12 (m, 1H); 2.56 (m, 1H) 2.18 (m, 1H); 1.98 (m, 2H); 1.84 ppm (m, 1H).

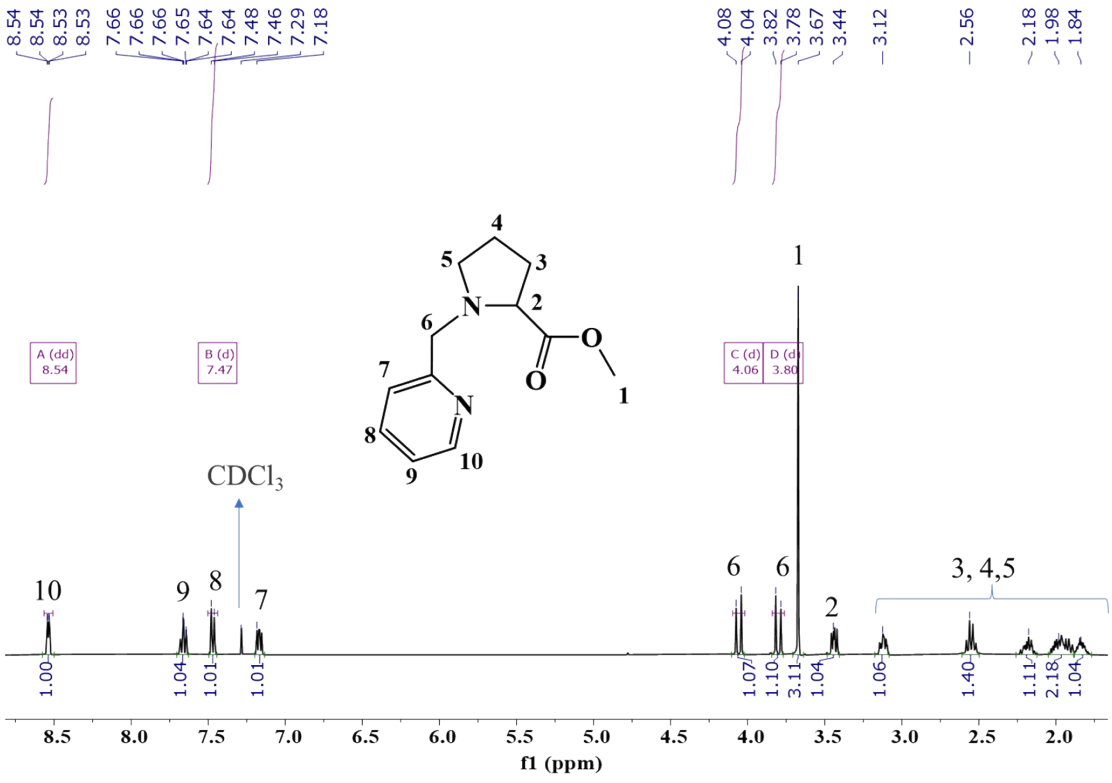

Fig. S1. ^{1}H NMR spectrum of compound (2) ($CDCl_3$, 400 MHz).

Synthesis of diphenyl(1-(pyridin-2-yl-methyl) pyrrolidin-2-yl) methanol (3)

Magnesium turnings (0.653 g, 0.026 mol) were added to a 250 mL Schlenk flask. The flask was flame-dried and cooled to room temperature. To this flask, 30 mL of anhydrous THF were added, followed by the addition of 20 mg of iodine. After the iodine dissolved, 2.86 mL of benzyl bromide (0.026 mol) were added, and the reaction was stirred at room temperature until magnesium was fully consumed. Then, the reaction flask was immersed into an ice bath and 2.96g (0.013 mol) of (2) were added to the reaction mixture. After 1 hour at room temperature, the reaction was quenched with 10% HCl and was stirred for another hour. The reaction mixture was neutralized with sodium hydroxide solution (0.1 M) and extracted with dichloromethane (3 x 50 mL). The organic phases were mixed and dried with $MgSO_4$, filtered and the solvent was removed under reduced pressure. The product was purified by column chromatography over silica gel using a 1:1 mixture of ethyl acetate and hexane as eluent, to give 1.88g (42% yield) of a light-yellow solid.

^{1}H NMR: (400 MHz, $CDCl_3$): δ 8.45 (d, J=4.9Hz, 1H); 7.71 (d, J=8.1 Hz, 2H); 7.60 (m, 3H); 7.32 (m, 4H); 7.19 (m, 1H); 7.10 (m, 3H); 5.05 (br, 1H) 4.11 (s, 1H); 3.41 (m, 2H); 3.02 (m, 1H); 2.58 (m, 1H); 2.00 (m, 1H); 1.81 (m, 1H); 1.69 ppm (m, 1H).

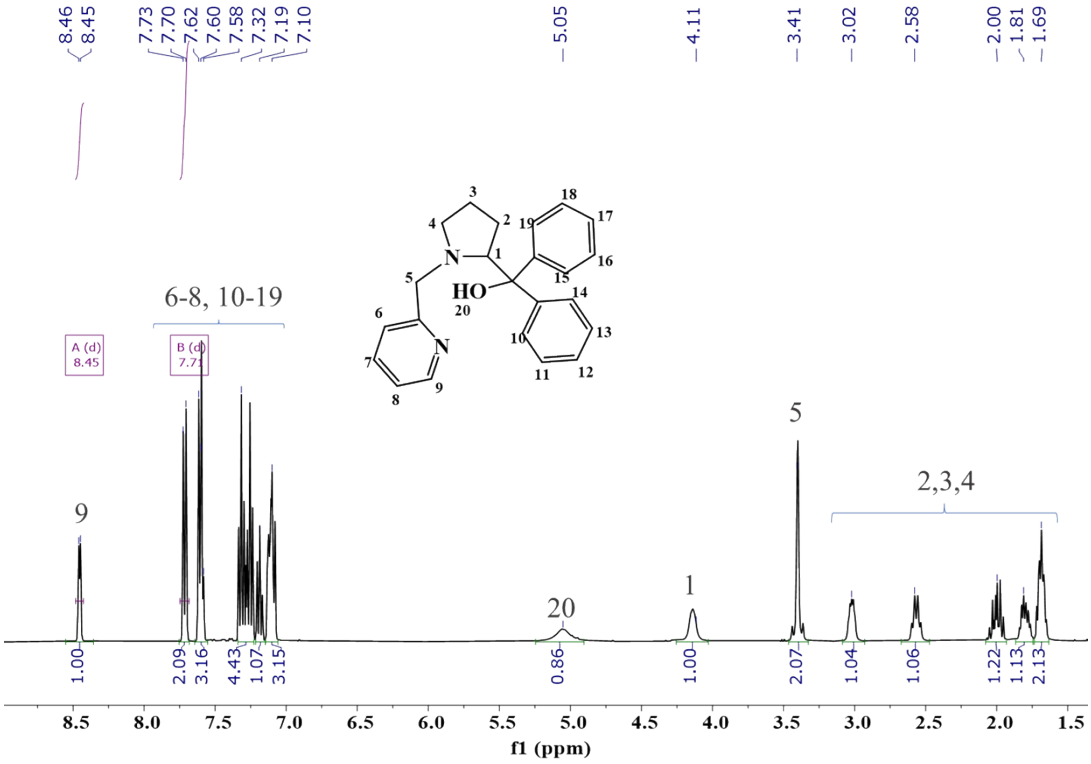

Fig. S2. ^{1}H NMR spectrum of compound (3). ($CDCl_3$, 400 MHz).

Synthesis of 2-((2-(azido bis-phenylmethyl)pyrrolidin-1-yl)methyl)pyridine (4)

To 40 mL of chloroform was added 1 g of compound (3) (0.270 mmol) and 1 g of sodium azide (1.538 mmol). This solution was kept in an ice bath and then, a 75% solution of H_2SO_4 was added dropwise to the reaction mixture. The latter was kept under stirring at 12 °C for 24 hours. After this period the reaction was neutralized with concentrated sodium bicarbonate solution and extracted with dichloromethane (3 x 30 mL). The organic phases were mixed and dried with $MgSO_4$, filtered and the solvent was removed under reduced pressure to obtain 1.07g of (4) as a brown oil (yield >99%).

FTIR (KBr pellet, cm^{-1}): 2108 cm^{-1} , s [ν (N=N=N)]

^1H NMR: (400 MHz, $CDCl_3$): δ 8.45 (dd, J= 1.4 Hz, 1H); 7.62 (m, 1H); 7.52 (m, 2H); 7.47 (m, 2H); 7.38-7.20 (m, 8H); 7.12 (m, 1H); 4.20 (dd, J= 3.9 Hz, 1H); 3.90 (d, J= 14.4 Hz, 1H); 3.66 (d, J= 14.4 Hz, 1H); 2.90 (m, 1H); 2.43 (m, 1H); 2.12 (m, 1H);1.88 (m, 1H); 1.63 (m, 1H); 1.40 ppm (m, 1H).

^{13}C NMR: 160.30; 148.30; 142.19; 141.80; 136.40; 128.01; 127.90; 127.42; 127.37; 122.81; 121.70; 77.25; 76.47; 72.71; 64.27; 57.71; 31.69; 23.32 ppm.

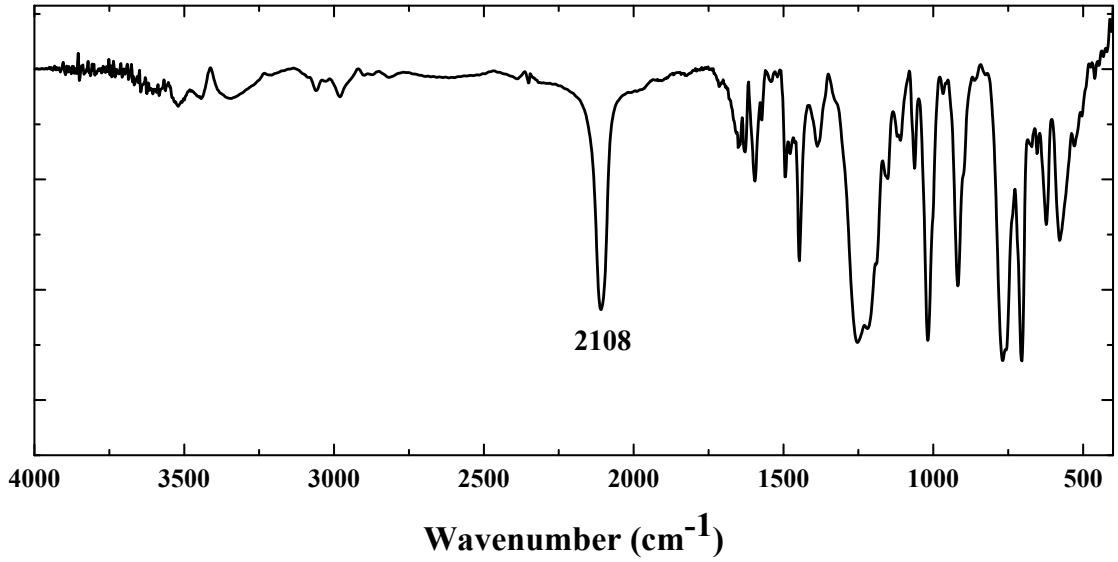

Fig. S3. FTIR spectrum of compound (4) in KBr disk. The spectrum shows the intense band at 2108 cm^{-1} characteristic of azide.

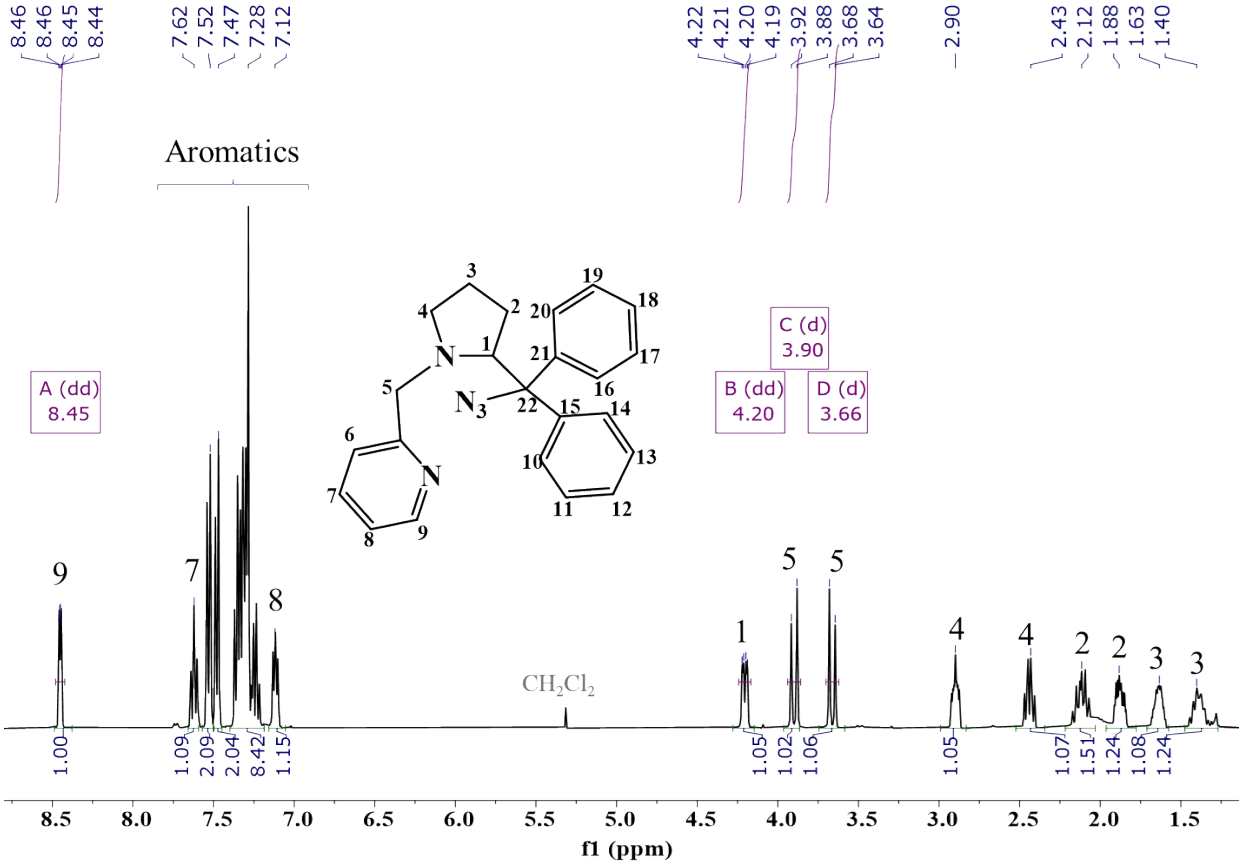

Fig. S4. ^{1}H NMR spectrum of compound (4). ($CDCl_3$).

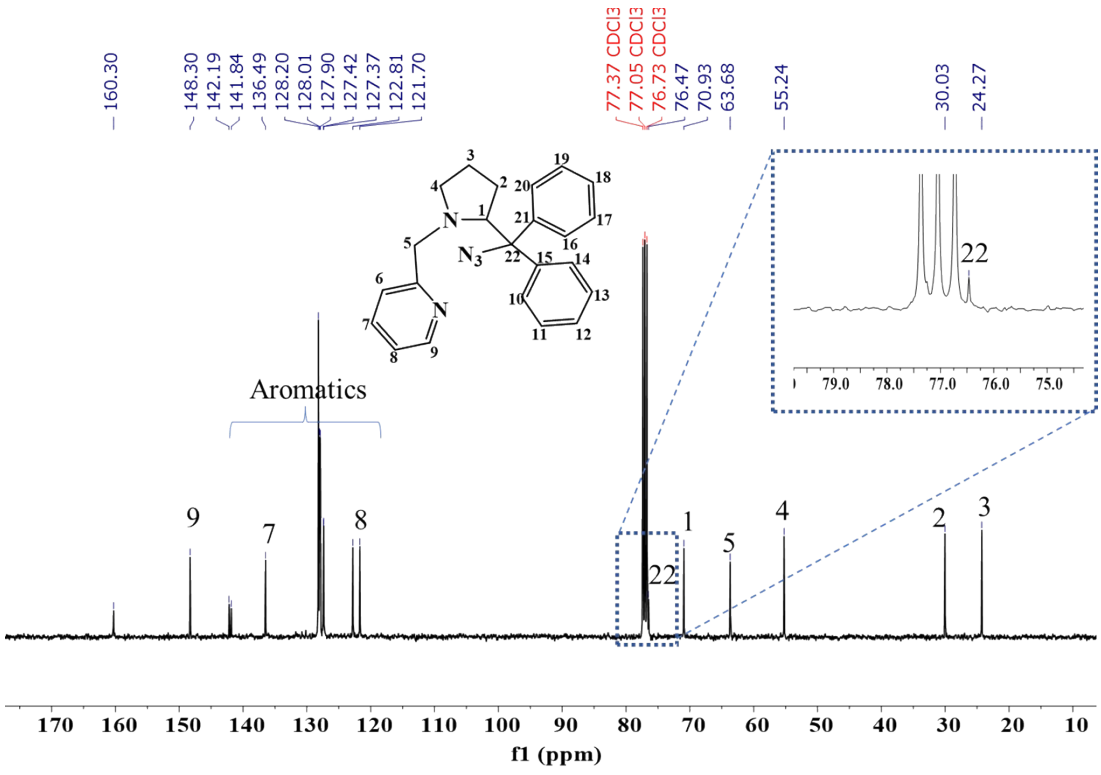

Fig. S5. ^{13}C NMR spectrum of compound (4). ($CDCl_3$).

Synthesis of ligands PTPh, PTB and PTP

To a 50 mL flask was added 1g of azide (4) (27 mmol) and 20 mL of acetonitrile under nitrogen atmosphere. Then, 0.270 mmol of the alkyne (ethynylbenzene, 4-pentyn-1-ol or 1-hexyne) were added to the flask, followed by the addition of 33 mg of $CuSO_4.5H_2O$ (5 mol%), 53 mg of sodium ascorbate (10 mol%) and 1 mL of water. The solution was kept under argon atmosphere at room temperature for 24 hours. Then, 15 mL of water were added to the reaction and an extraction with dichloromethane (3 x 30 mL) was performed. The organic phases were mixed and dried with $MgSO_4$, filtered and the solvent was removed under reduced pressure. The products were purified by column chromatography over silica gel using a 1:1 solution of ethyl acetate and hexane as eluent obtaining yields of 82% for PTPh, 76% for PTB and 57% for PTP.

PTPh, FTIR (KBr pellet, cm^{-1}): 3058 ν (C-H) sp^2; 2964, 2875, 2813 ν (C-H) sp^3; 1590, 1568 ν(C=N); 1491, 1481, 1448, 1432 ν (C=C); 1072 ν(C-N); 695, 763 $\delta_{\text{out of plane}}$ (=C-H).

PTPh, ^{1}H NMR: (400 MHz, acetone-d_6): δ 8.54 (s, 1H); 8.44 (d, J= 4.7 Hz, 1H); 7.90 (m, 2H); 7.60 (m, 5H); 7.41-7.26 (m, 9H); 7.13 (m, 1H); 6,99 (d, J= 7,8 Hz, 1H); 5.26 (dd, J= 9.5 Hz, 1H); 4.20 (d, J= 13.9 Hz, 1H); 3.71 (d, J= 13.9 Hz, 1H); 2.52 (m, 1H); 2.44 (m, 2H); 1.86 (m, 1H) 1.37 (m, 1H); 0.25 ppm (m, 1H).

PTPh, ^{13}C NMR: δ 160.29; 148.38; 145.36; 141.06; 140.21; 135.71; 131.19; 130.09; 128.37; 127.60; 127.44; 127.30; 127.20; 127.16; 125.08; 122.75; 122.15; 121.28; 77.56; 69.04; 62.77; 54.64; 30.34; 23.09 ppm.

PTPh, HRMS: $[MH]^+$: 472.2520 (found); 472.2501 (calc. for $C_{31}H_{30}N_5$)

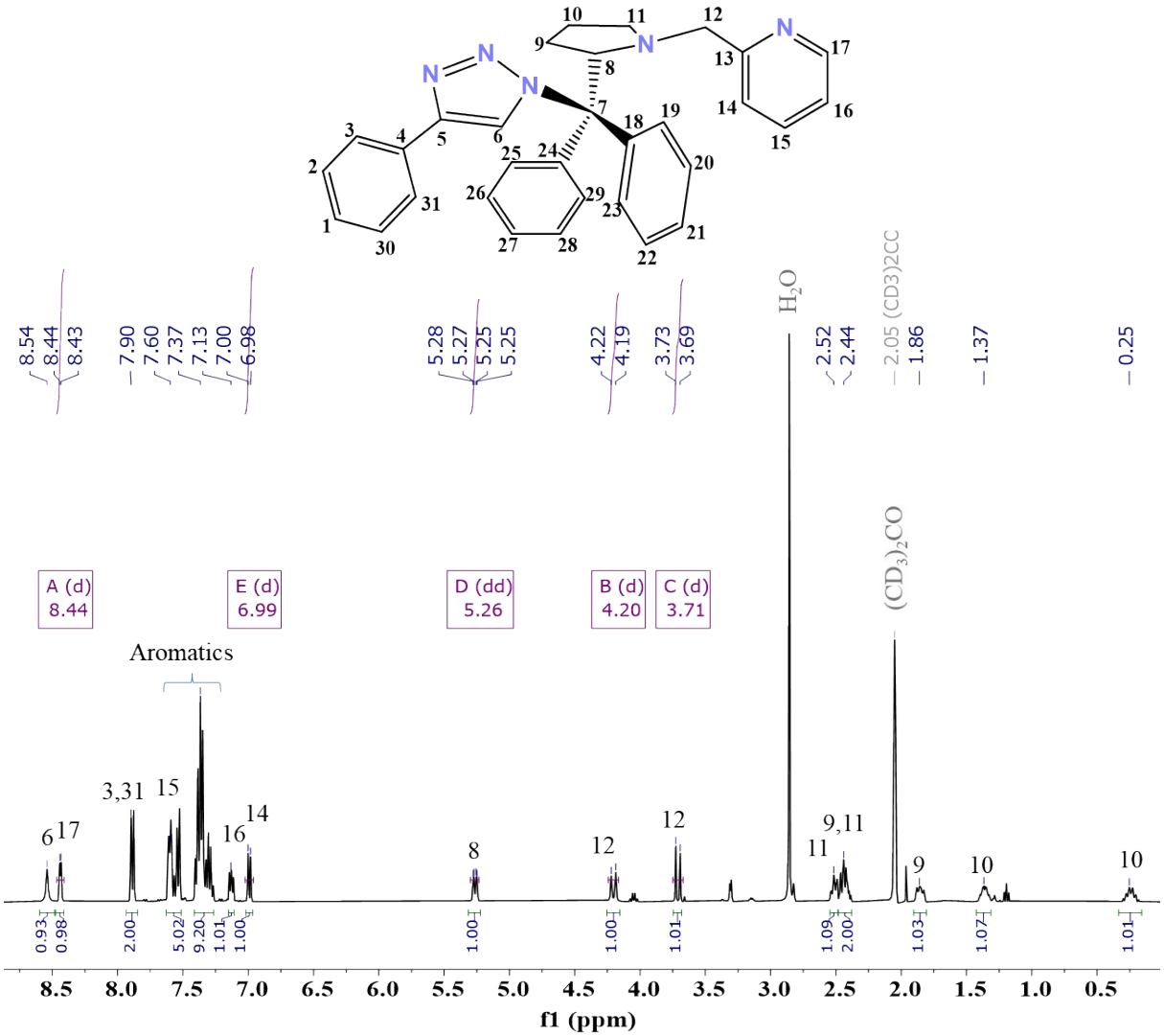

Fig. S6. ^{1}H NMR spectrum of ligand PTPh in $(CD_3)_2CO$, 400 MHz.

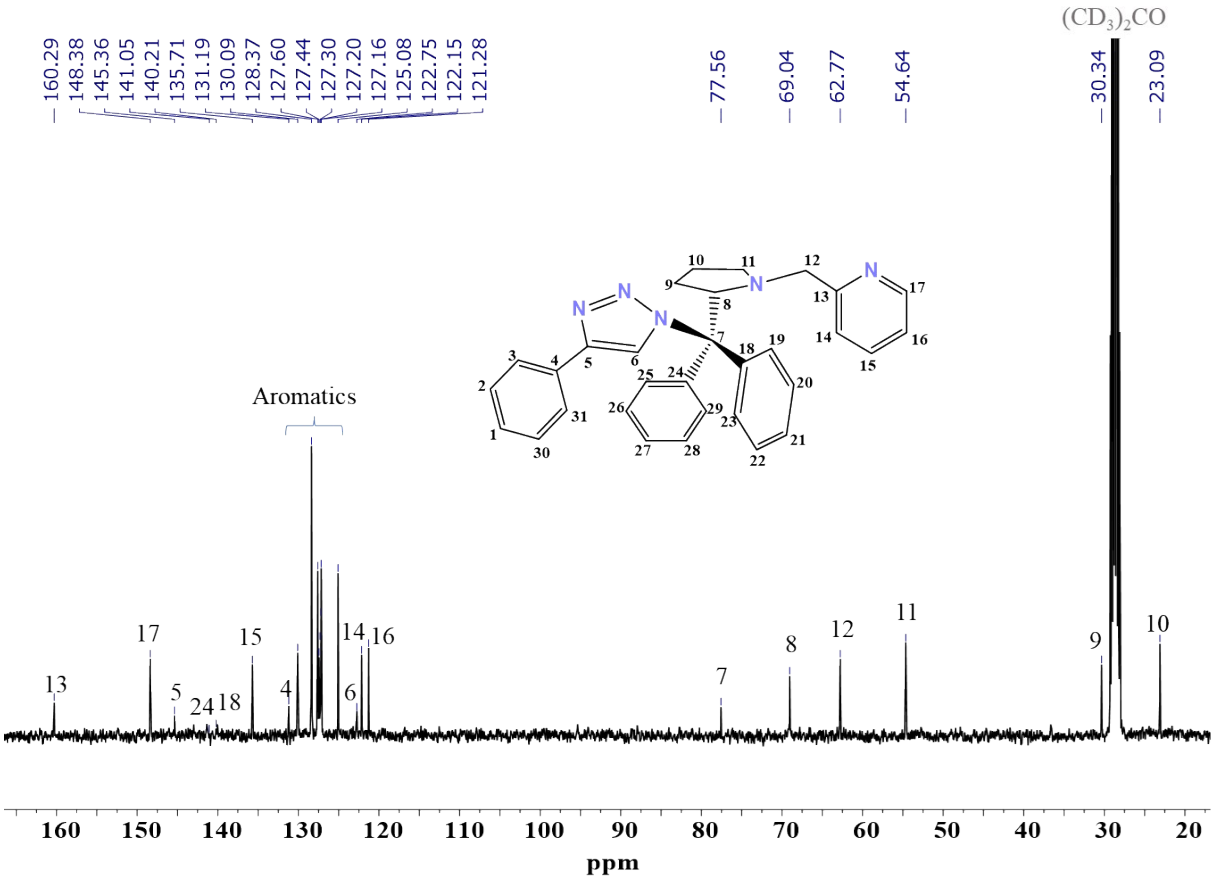

Fig. S7. ^{13}C NMR spectrum of ligand PTPh in $(CD_3)_2CO$, 400MHz.

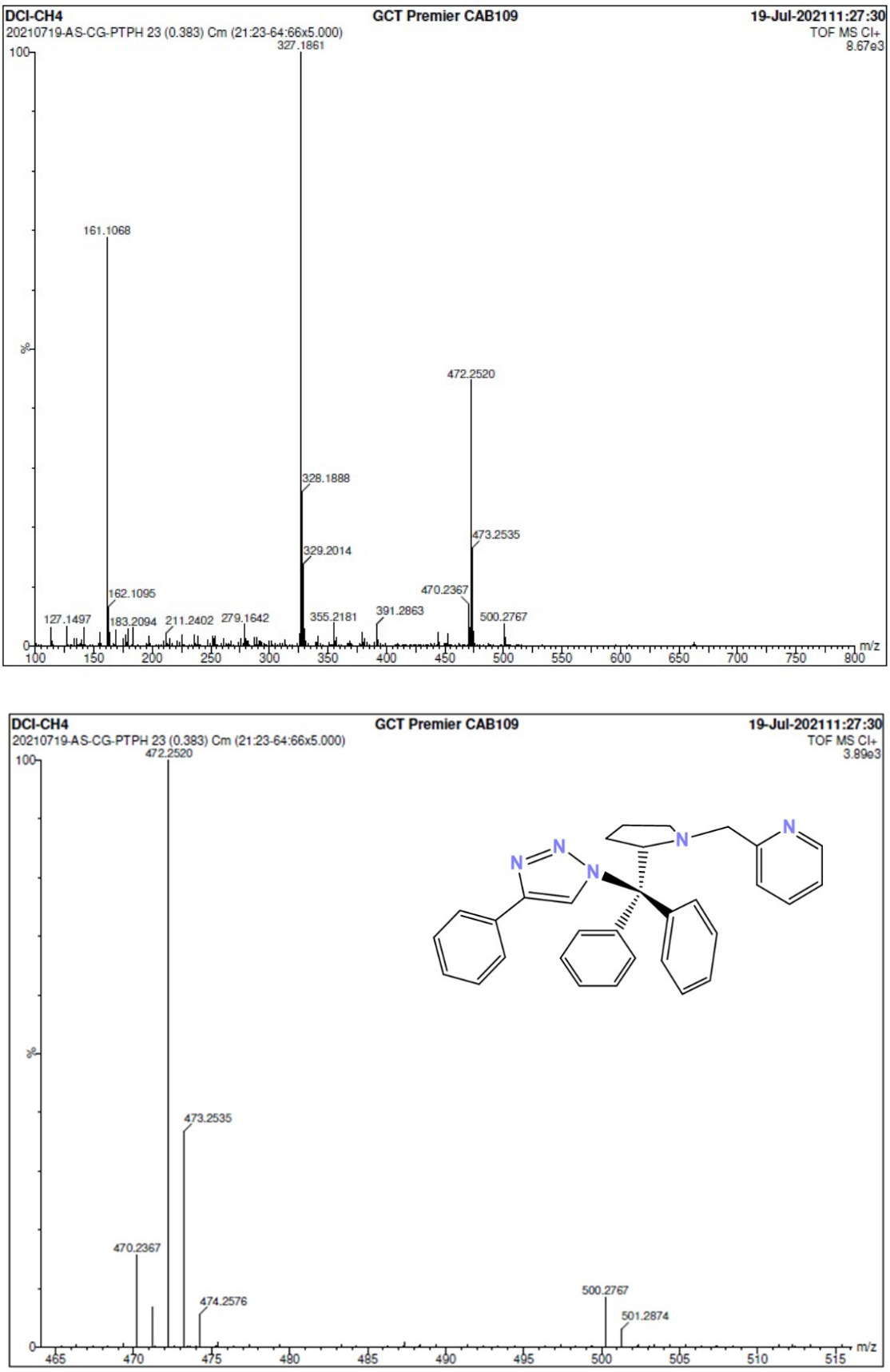

Fig. S8. ESI mass of ligand PTPh in methanol.

PTB, FTIR (KBr pellet, cm^{-1}): 3059 ν(C-H) sp^2; 2953, 2958, 2870, 2808 ν(C-H) sp^3; 1590, 1568 ν(C=N); 1493, 1474, 1447, 1433 ν(C=C); 1042 ν(C-N); 703, 754 $\delta_{\text{out of plane}}$(=C-H).

PTB, ^{1}H NMR: (400 MHz, acetone-d_6): , δ 8.41 (d, J= 3.5 Hz, 1H); δ 7.71 (s, 1H); 7.61 (t, 1H); 7.54 (m, 2H); 7.41 (m, 2H); 7.37-7.27 (m, 6H); 7.14 (m, 1H); 6.92 (d, J=7.8 Hz, 1H); 5.16 (dd, J= 2.9 Hz, 1H); 4.16 (d, J= 13.8 Hz, 1H); 3.64 (d, J= 13.8 Hz, 1H); 2.63 (t, J= 7.6 Hz, 2H); 2.51 (m, 1H) 2.404 (m, 2H);1.80 (m, 1H); 1.57 (quin, 2H); 1.36 (m, 1H); 1.31 (m, 2H); 0.86 (t, J= 7,9 Hz, 3H); 0,24 ppm (m, 1H).

PTB, ^{13}C NMR: δ 160.69; 148.54; 146.14; 141.93; 140.48; 135.97; 130.47; 128.64; 127.77; 127.69; 127.40; 127.31; 123.43; 122.48; 121.54; 77.28; 69.64; 63.35; 55.00; 31.60; 30.73; 25.03; 23.45; 21.90; 13.22 ppm.

PTB, HRMS: $[MH]^+$: 452.2809 (found); 452.2814 (calc. for $C_{29}H_{34}N_5$)

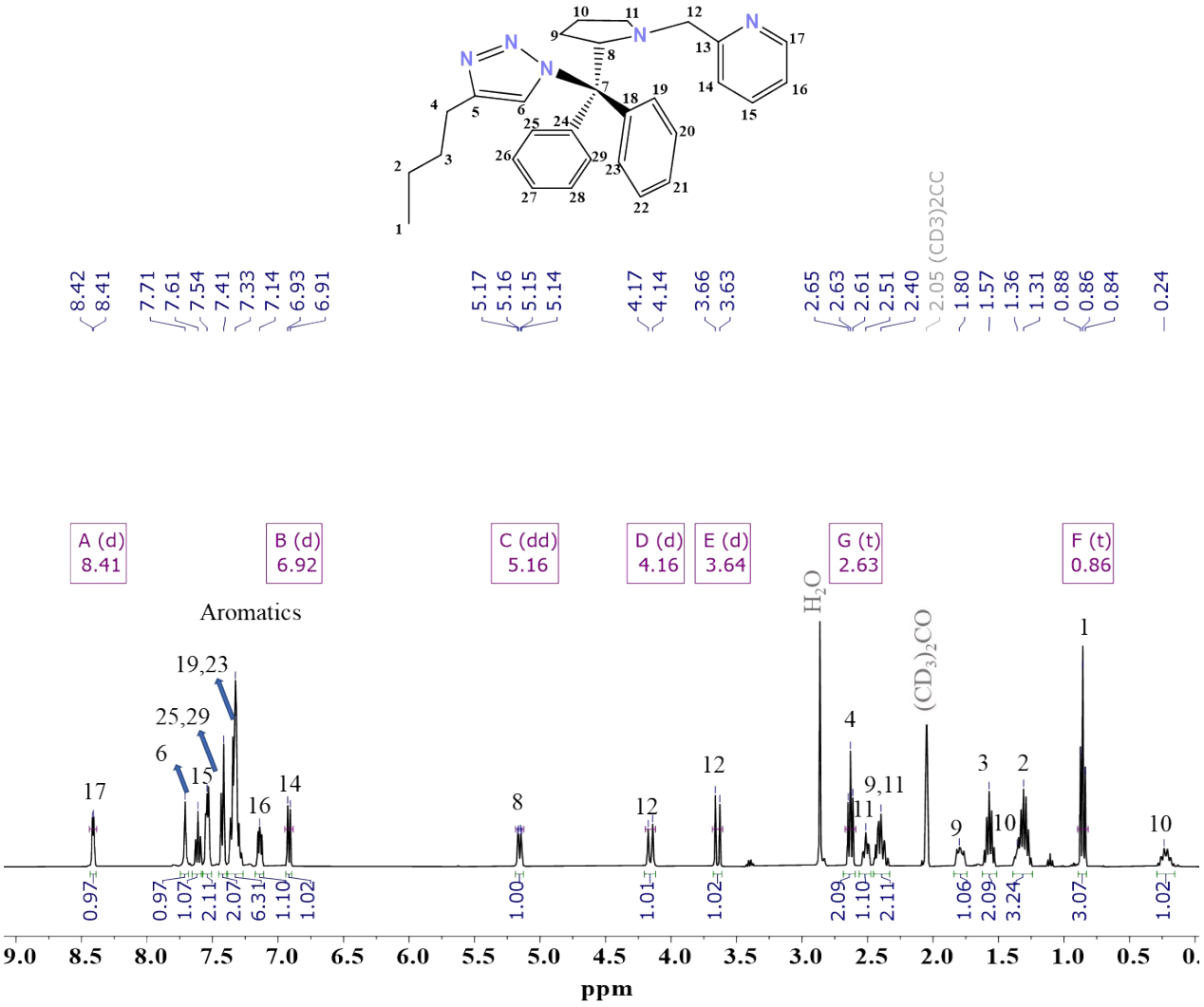

Fig. S9. ^{1}H NMR spectrum of ligand PTB in $(CD_3)_2CO$, 400 MHz.

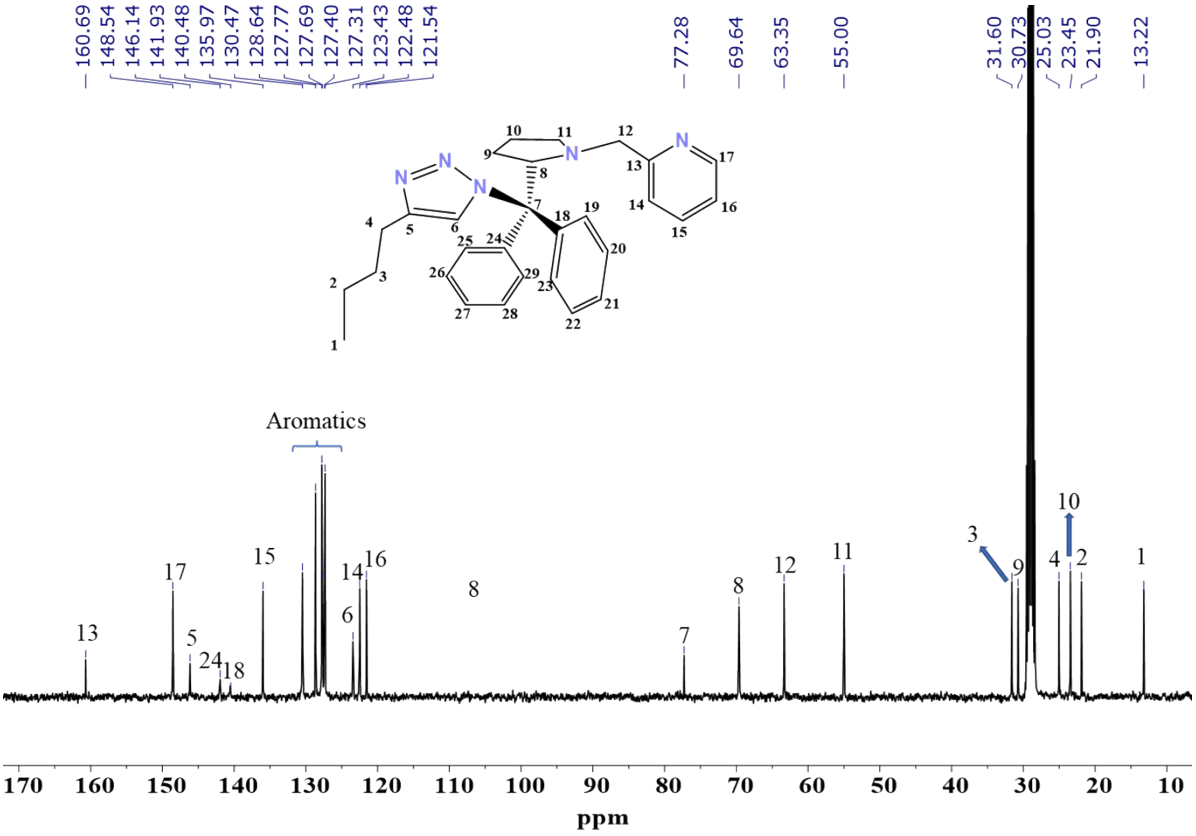

Fig. S10. ^{13}C NMR spectrum of ligand PTB in $(CD_3)_2CO$, 400MHz.

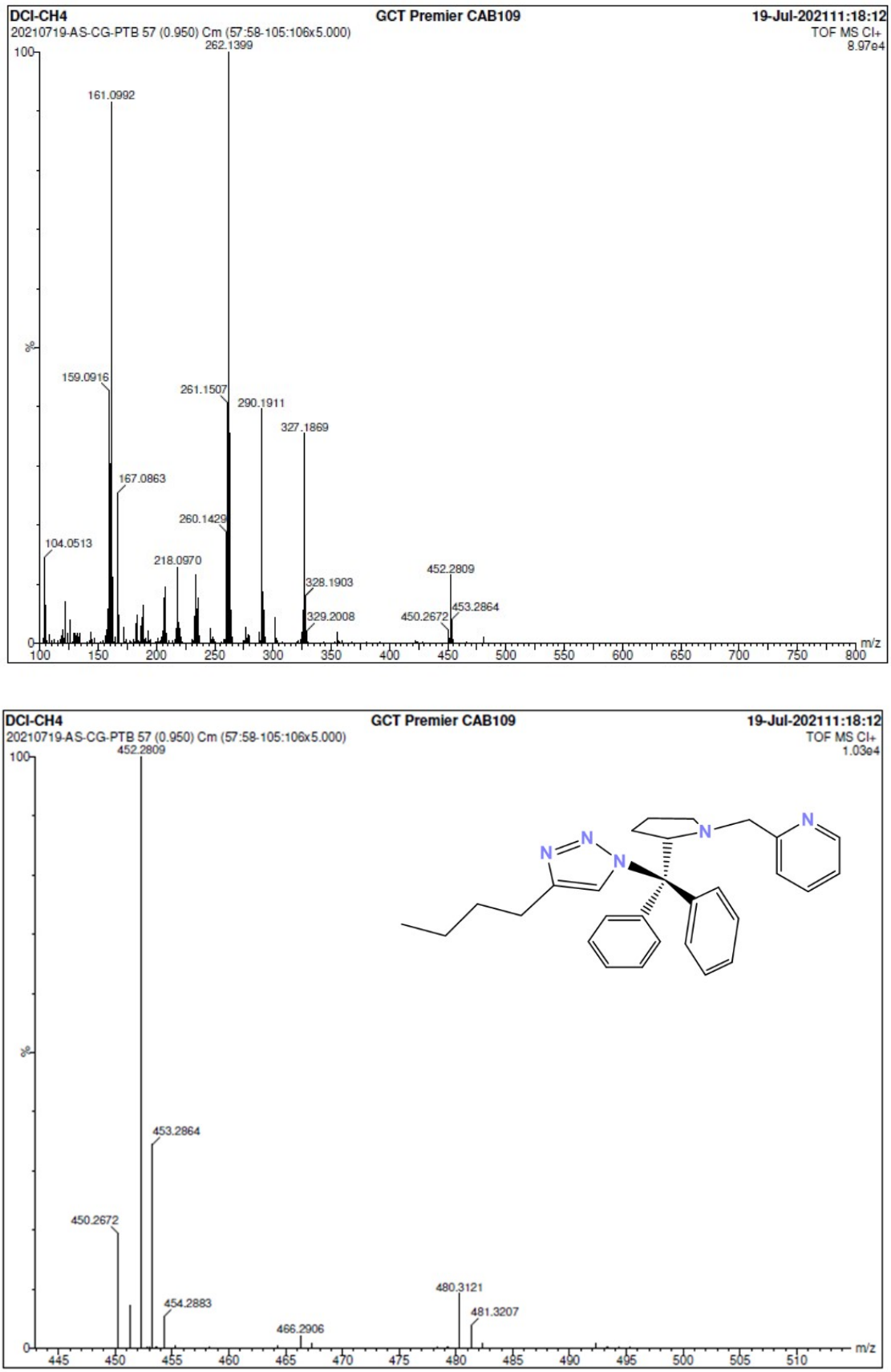

Fig. S11. ESI mass of ligand PTB in methanol.

PTP, FTIR (KBr pellet, cm^{-1}): 3380 ν(O-H); 3063 ν(C-H) sp^2; 2952, 2875, 2834 ν(C-H)sp^3; 1600, 1577 ν(C=N); 1500, 1483, 1455, 1441 ν(C=C); 1054 ν(C-N); 703, 754 $\delta_{\text{out of plane}}$ (=C-H).

PTP, ^{1}H NMR: (400 MHz, acetone-d_6): δ 8.41 (d, J= 4.9 Hz, 1H); 7.73 (s, 1H); 7.62 (t, 1H); 7.53 (m, 2H); 7.42 (m, 2H);7.37-7.27 (m, 6H); 7.14 (m, 1H); 6.91 (d, J= 7.7 Hz, 1H); 5.17 (dd, J= 2.8 Hz, 1H); 4.17 (d, J= 13.8 Hz, 1H); 3.65 (d, J= 13.8 Hz, 1H); 3.54 (t, J= 6.4 Hz, 2H); 2.90 (m, 1H) 2.72 (t, J= 7.5 Hz, 2H); 2.52 (m, 1H); 2.40 (m, 2H); 1.80 (m, 3H); 1.35 (m, 1H); 0.24 ppm (m, 1H).

PTP, ^{13}C NMR: δ 160.69; 148.54; 146.14; 141.93; 140.48; 135.97; 130.47; 128.64; 127.77; 127.69; 127.40; 127.31; 123.43; 122.48; 121.54 ppm.

PTP, HRMS: $[MH]^+$: 454.2607 (found); 454.2606 (calc. for $C_{28}H_{32}N_5O$)

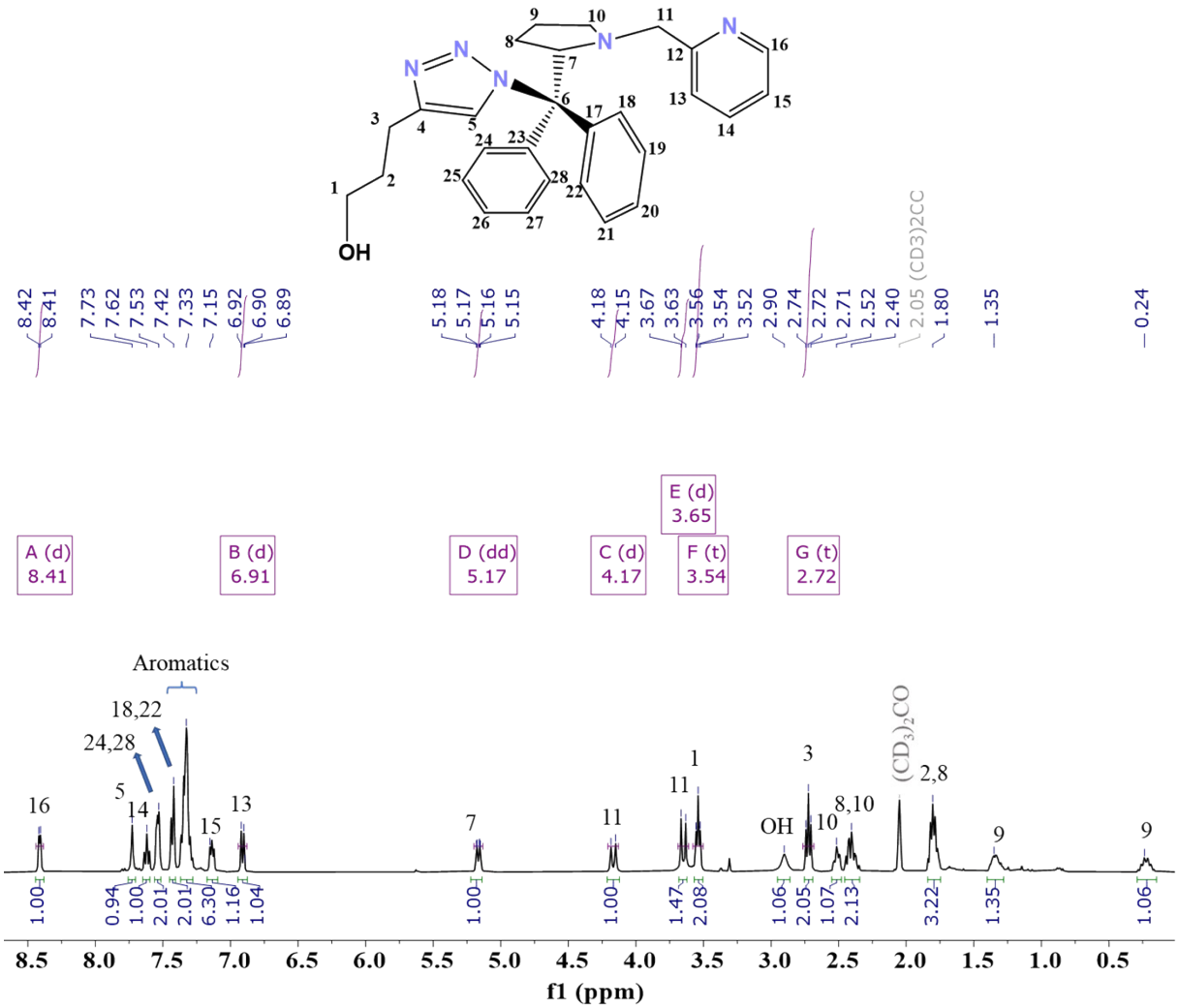

Fig. S12. ^{1}H NMR spectrum of ligand PTP in $(CD_3)_2CO$, 400MHz.

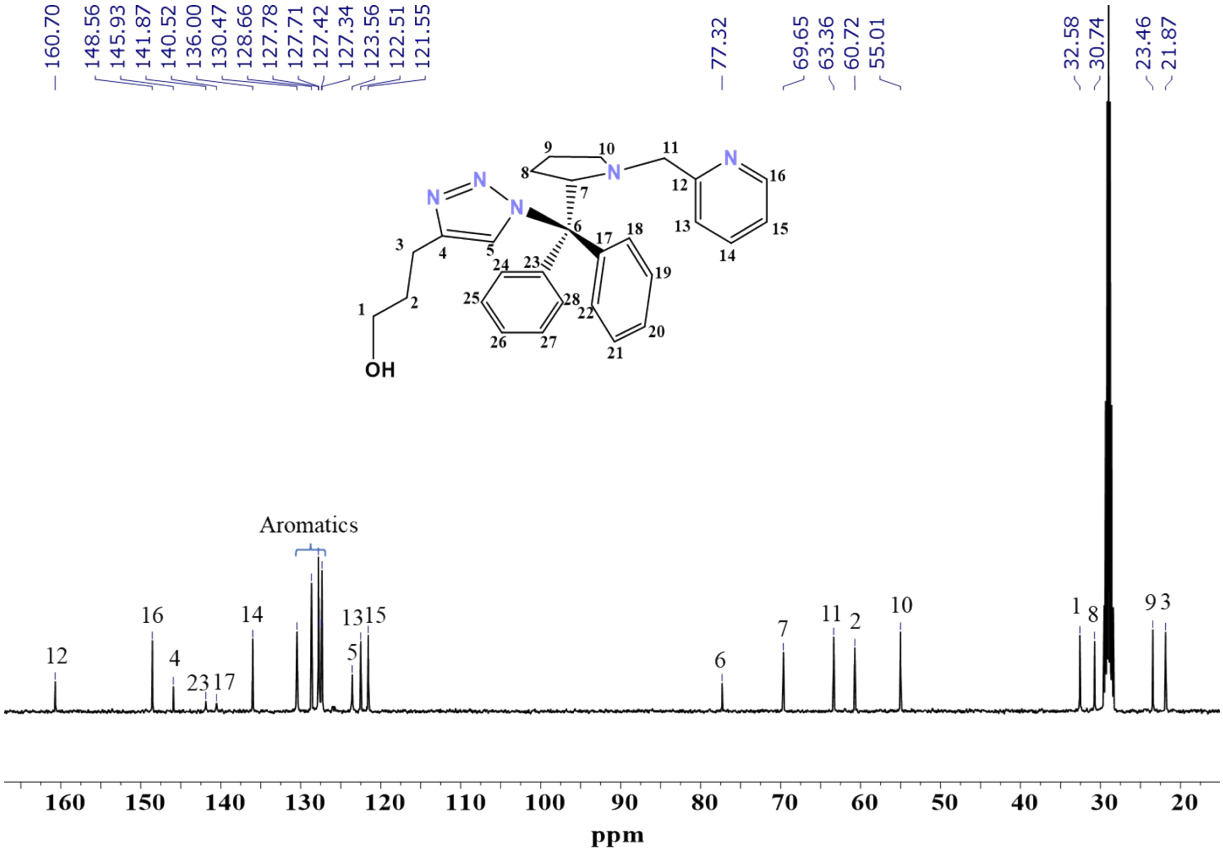

Fig. S13. ^{13}C NMR spectrum of ligand PTP in $(CD_3)_2CO$, 400MHz.

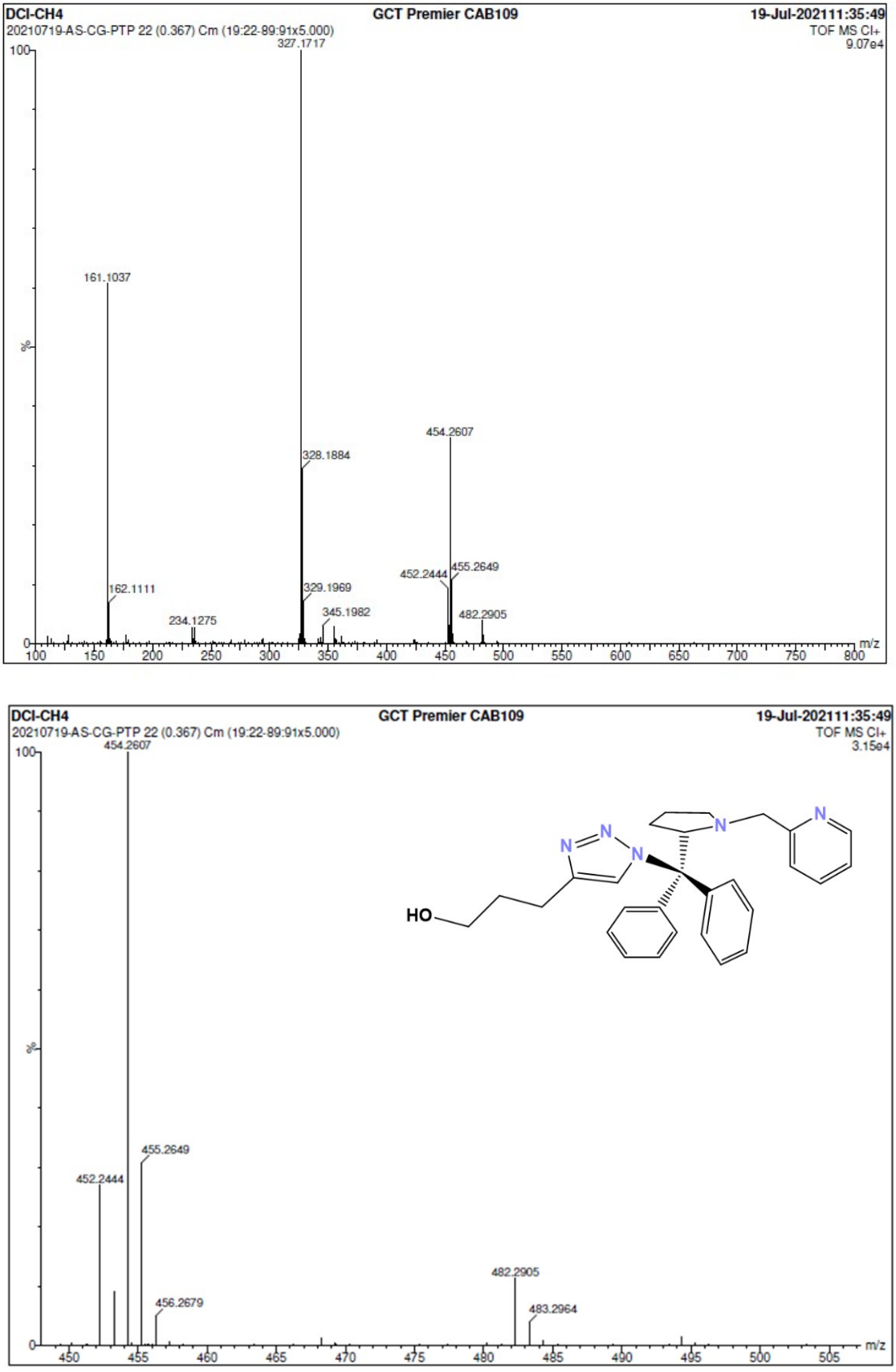

Fig. S14. ESI mass of ligand PTP and full scale in methanol.

3. Catalytic experiments

- Reduction of the Cu^{2+} complexes with sodium ascorbate.

The reduction was performed *in situ* in a quartz cuvette with a young tap. To the cuvette, 3 mL of a 1 mM solution of the copper complexes in methanol was added. This solution was deaerated by bubbling argon into it for 15 minutes. After this period, 150 µl of a methanolic solution of sodium ascorbate (20 mM) was added to the copper complex solution.

- NO generation from NO_2^-

To a 10 mL flask was added 3 mL of citrate buffer solution (0.1 M, pH=5), through which N_2 was bubbled for 15 minutes. After this period, 30 µmol of $FeSO_4.7H_2O$ and 30 µmol of EDTA (ethylenediaminetetraacetic acid) were added to it. The system was kept under N_2 and stirred for 5 minutes. In another Schlenk flask, connected with a tygon tube to the flask containing the ferrous complex, was added 1 mL of a methanolic solution of the copper complex (0.5mM, 0.5 µmol). Sodium nitrite (5 µmol), benzoic acid (10 µmol) and sodium ascorbate (5 µmol) were added to the copper complex with a syringe. After 10 minutes, the ferrous complex was analyzed by UV-Vis spectroscopy. The extinction coefficient used for the [Fe(EDTA)(NO)] complex refers to the operation conditions of the experiments and was determined by bubbling NO gas through the degassed 0.01 M Fe(EDTA) solution for 5 min and reading its absorbance at 432 nm. Blank determinations of NO recovery from reduction of nitrite by ascorbate under the gas flow conditions used in the reactions were carried out on methanolic solutions containing $NaNO_2$ (5mM), benzoic acid (10 mM) and sodium ascorbate (5 mmol) and yielded an average of 0% NO (as [Fe(EDTA)- (NO)] complex) after 10 min. The yields of NO reported are relative yields calculated on the basis of the effective recovery of NO in positive control experiments using 1mL of acetic acid containing different $NaNO_2$ concentrations (5, 4, 3, 2 and 1 mM) producing a calibration curve with R^2=0.977 (Fig.S57). The experiments were run in triplicate with high reproducibility.

4. Characterization of complexes CuPTPh, CuPTB and CuPTP

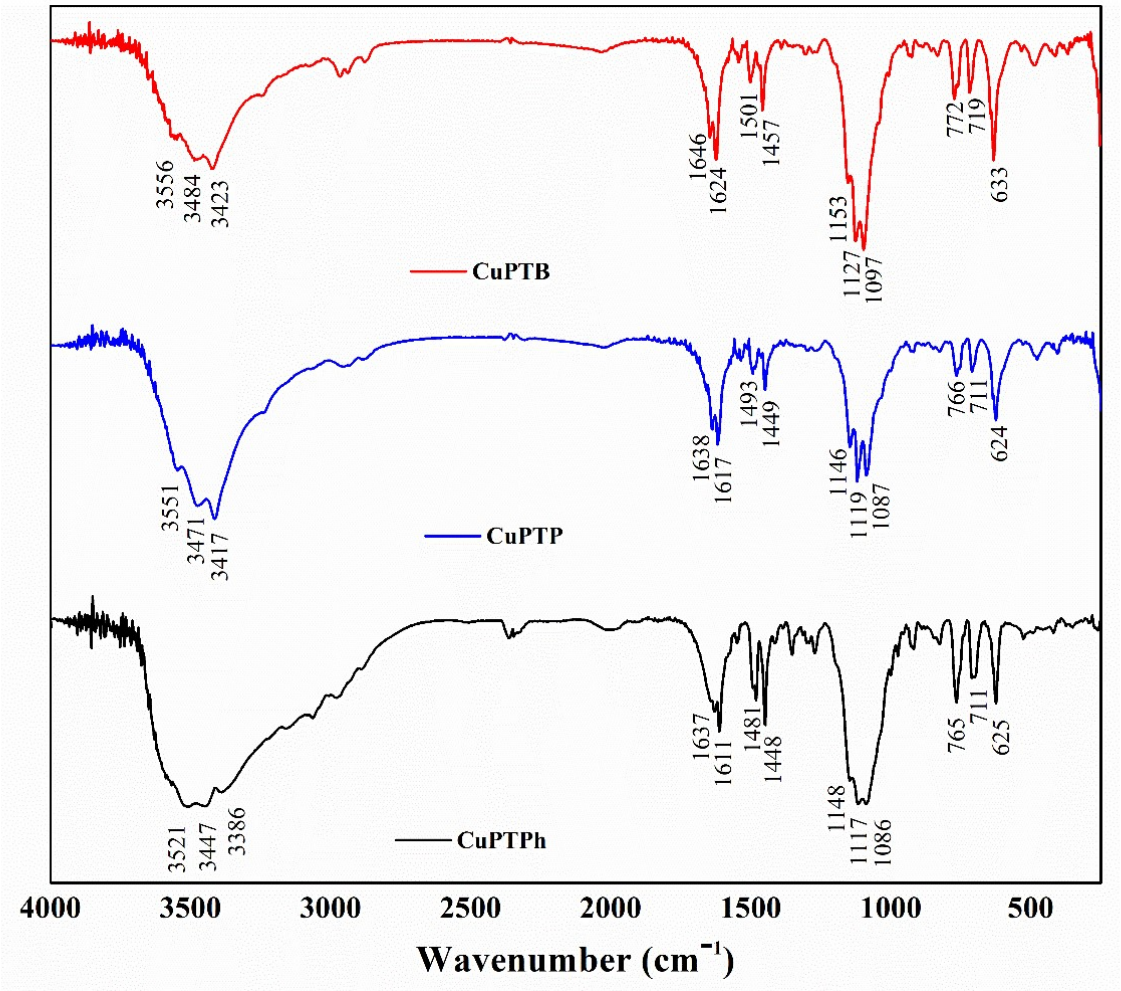

Fig. S15. FTIR spectrum of CuPTPh, CuPTB and CuPTP complexes in KBr disk.

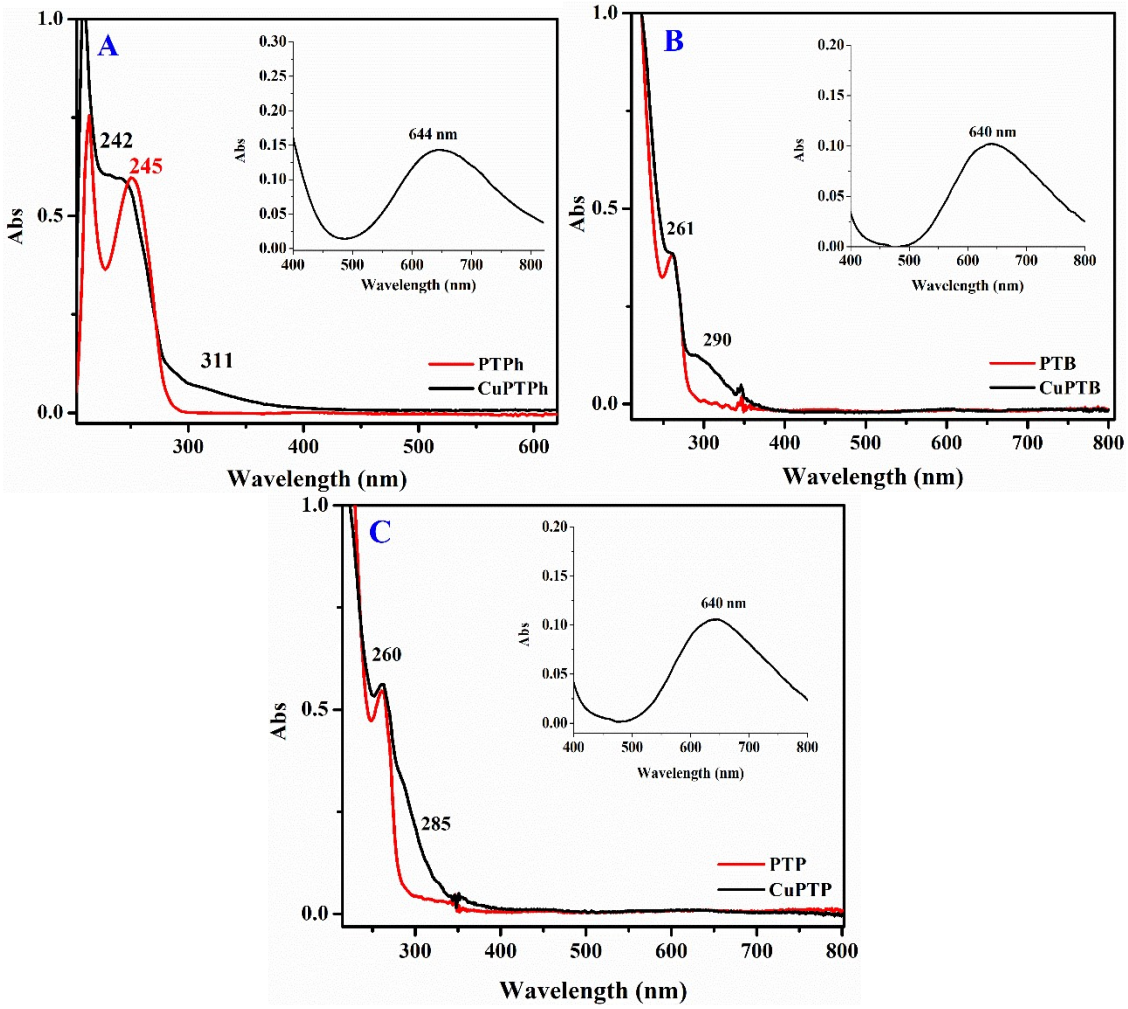

Fig. S16. UV-Vis spectra of CuPTPh, CuPTB and CuPTP complexes and comparation with yours respective ligands at same concentration. Spectra (inset) of transition d-d band (1 mmol. L^{-1}).

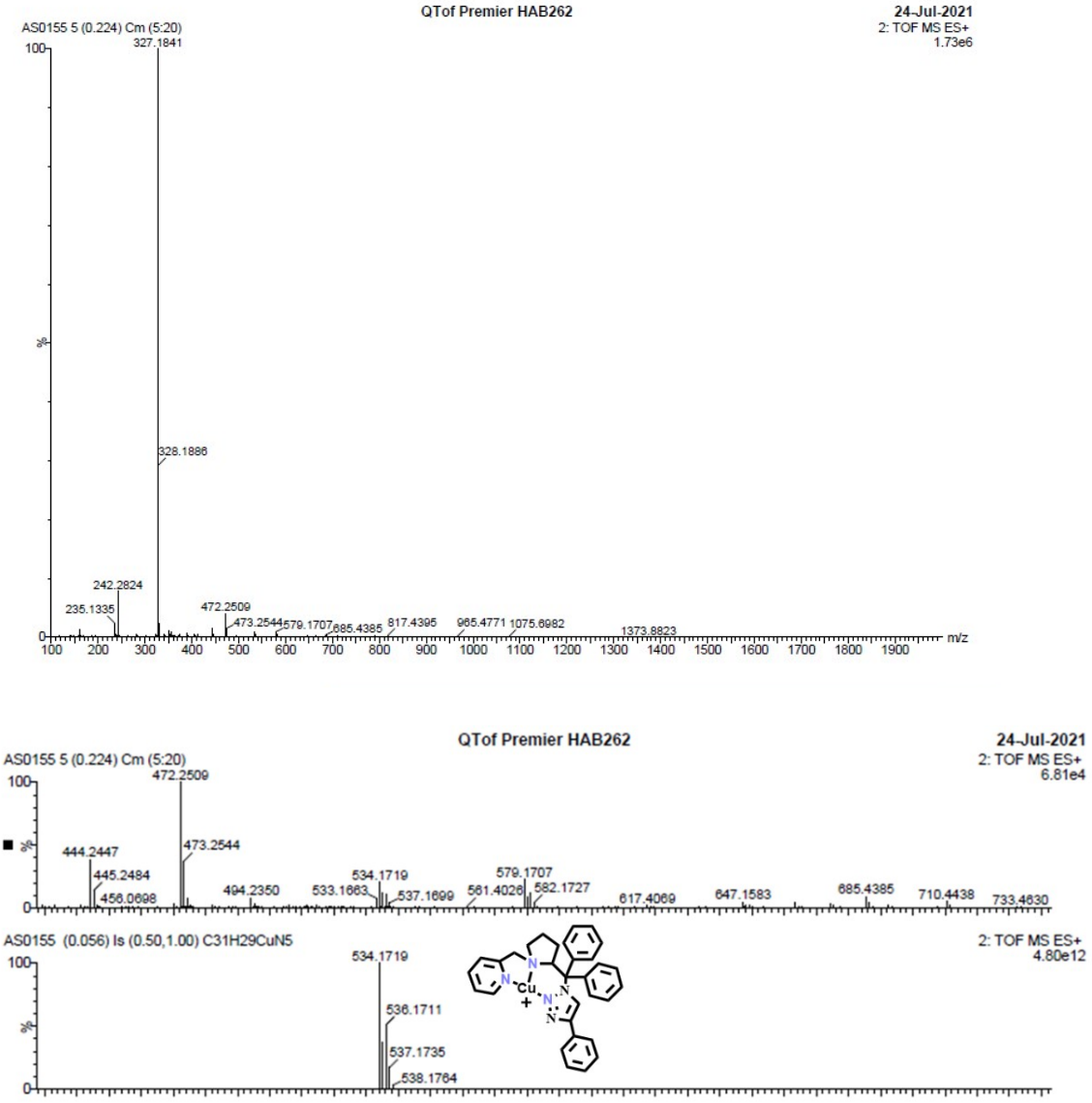

Fig. S17. ESI mass of complex CuPTPh in methanol.

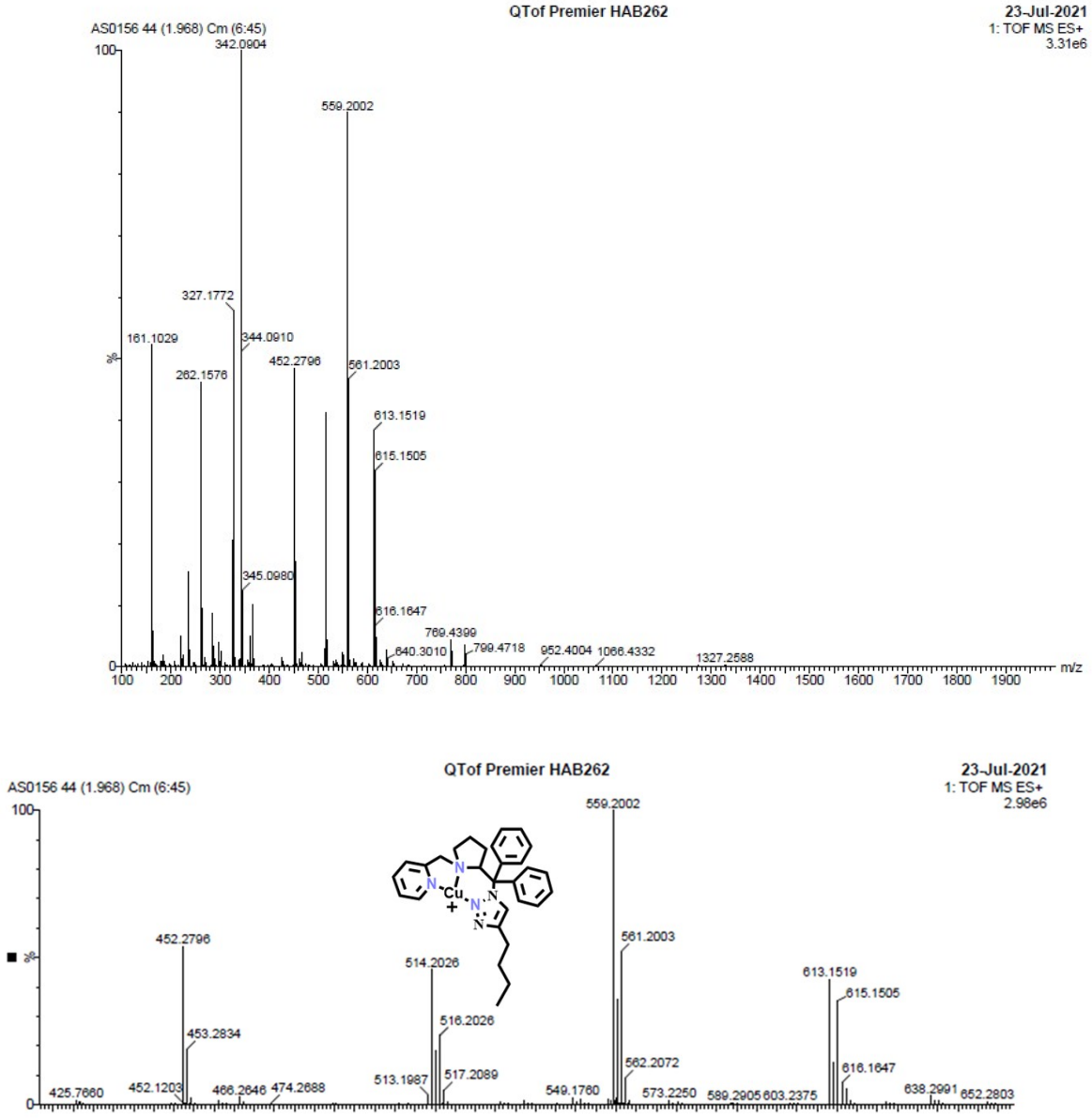

Fig. S18. ESI mass of complex CuPTB in methanol.

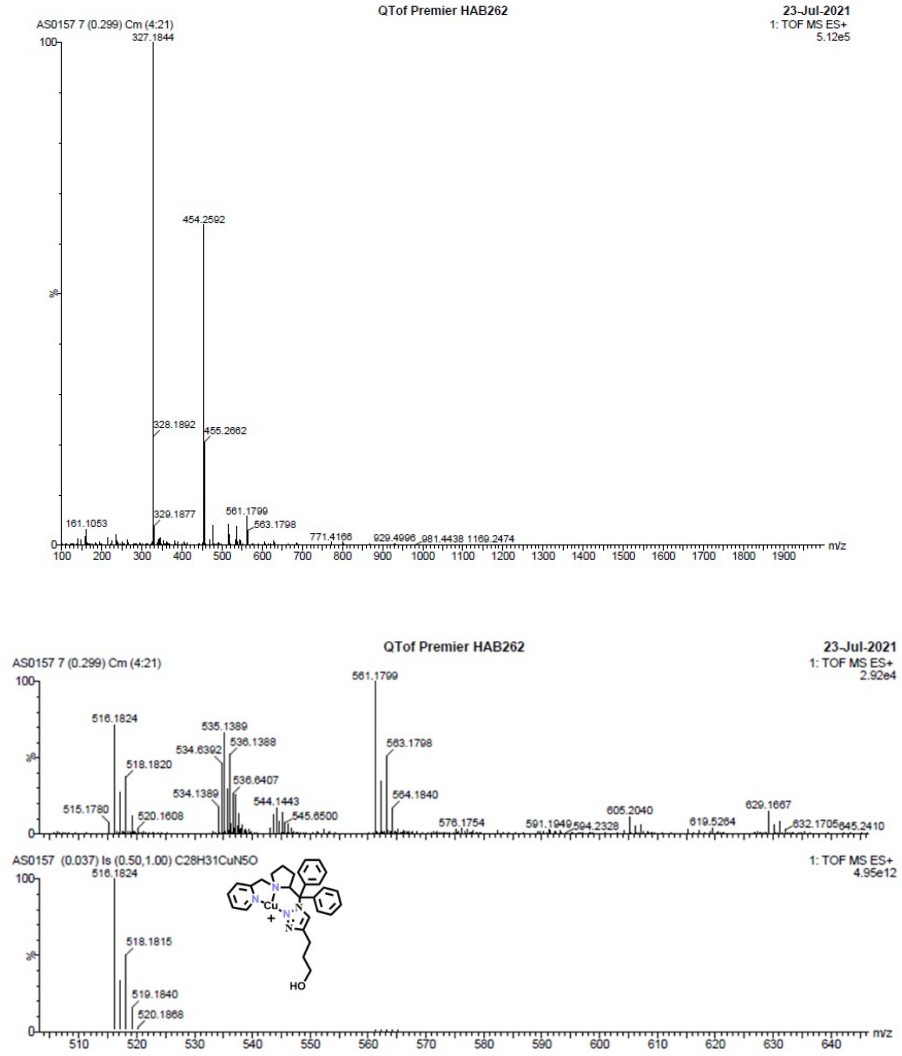

Fig. S19. ESI mass of complex CuPTP in methanol.

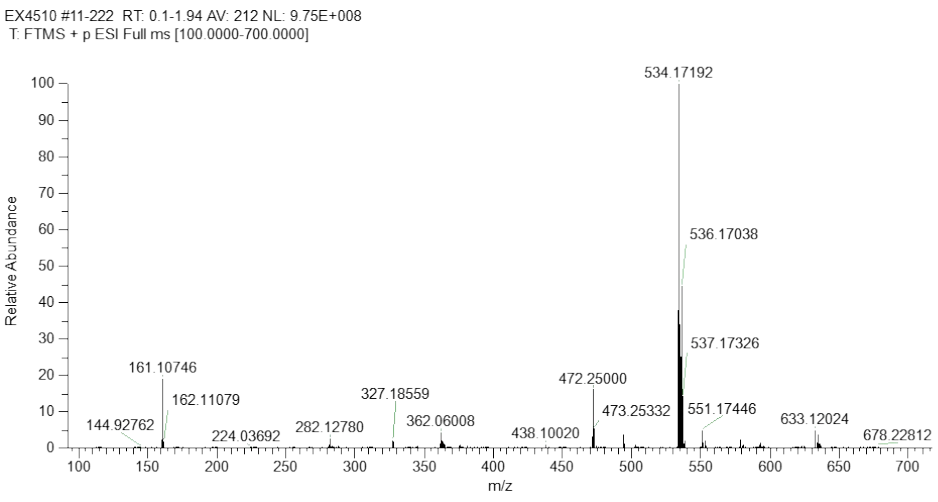

Fig. S20. ESI mass of complex CuPTPh(NO_2) in methanol.

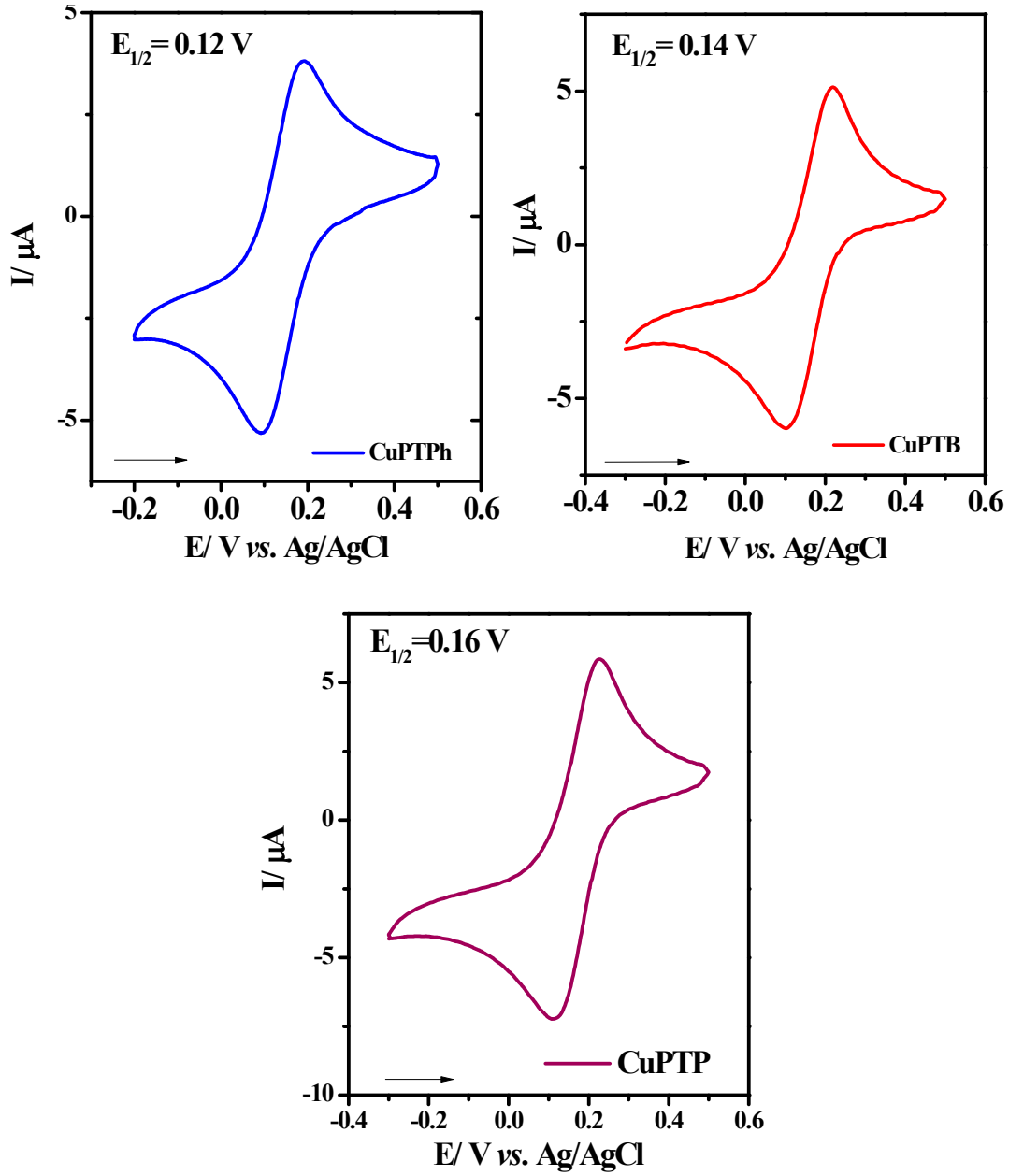

Fig. S21. Cyclic voltammetry of the 1mmol.L^{-1} solution of CuPTPh, CuPTB and CuPTP complexes in methanol containing PTBA 0.1 mol.L^{-1} as supporting electrolyte.

5. Nitrite coordination

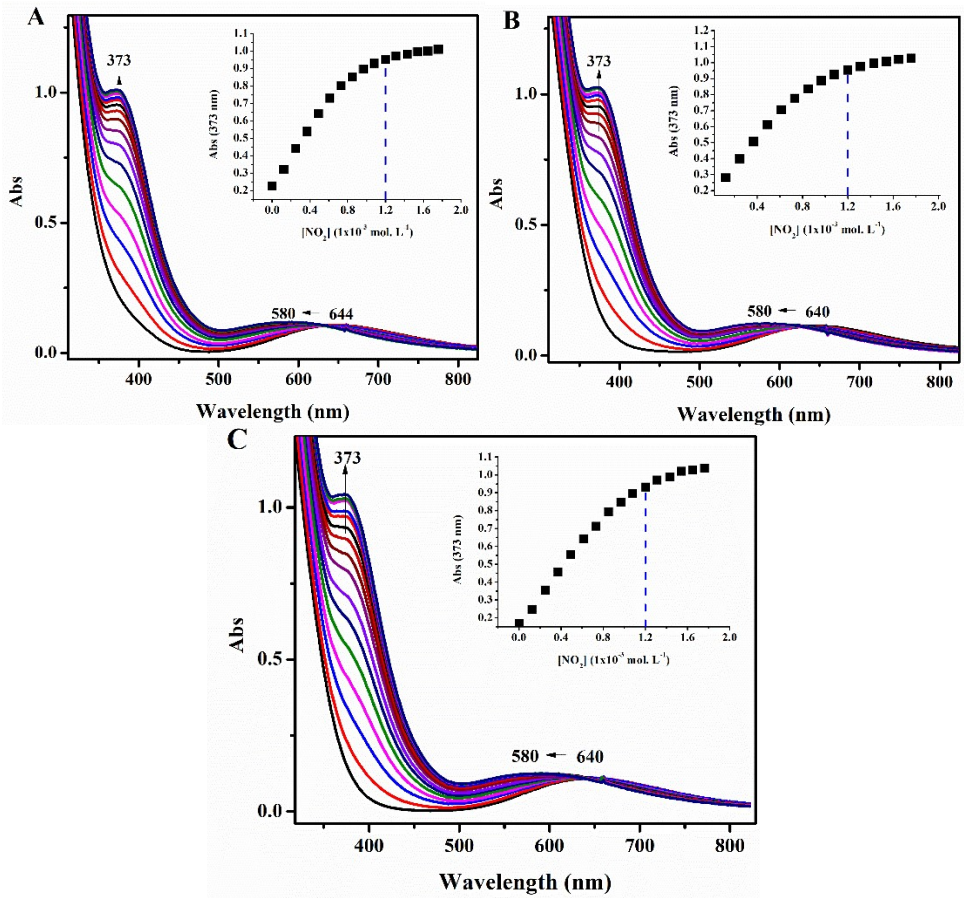

Fig. S22. UV-Vis spectra of the titration of complexes CuPTPh (A); CuPTB (B) and CuPTP (C) . All complexes were used at a concentration of 1.2 mmol. L^{-1} , with 0.1 mol. L^{-1} PTBA and nitrite. Nitrite addition additions of 10µL of 0.03 mol. L^{-1} were performed in methanol and the solution was at 25 °C. Plot (inset) of absorbance at 373 nm against nitrite concentration.

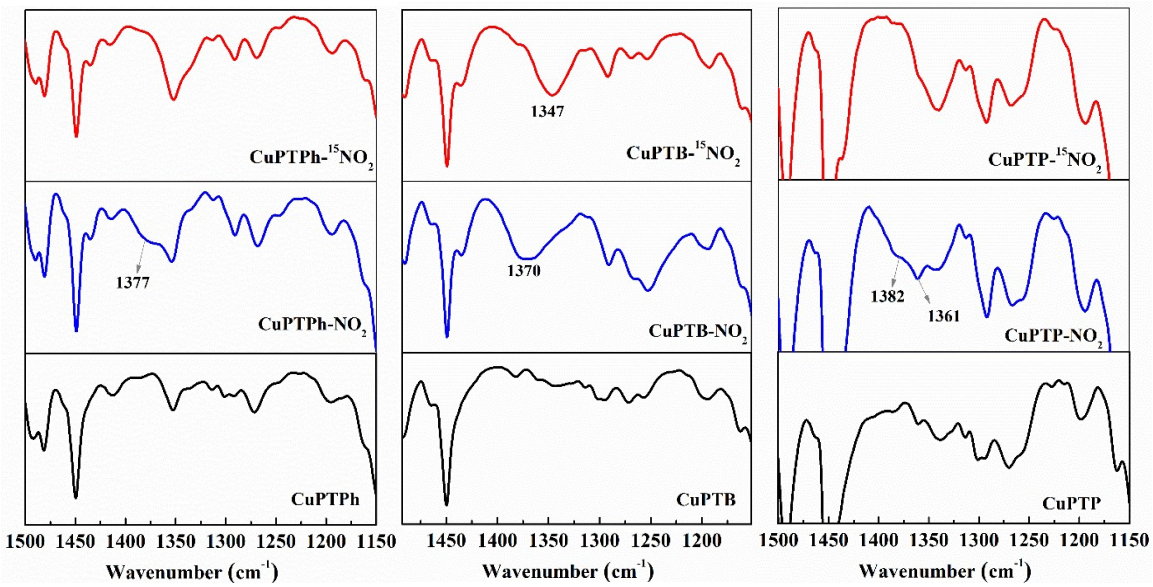

Fig. S23. FTIR spectra of CuPTPh, CuPTB and CuPTP complexes coordinated with NO_2^- and $^{15}NO_2^-$ using ATR-FTIR.

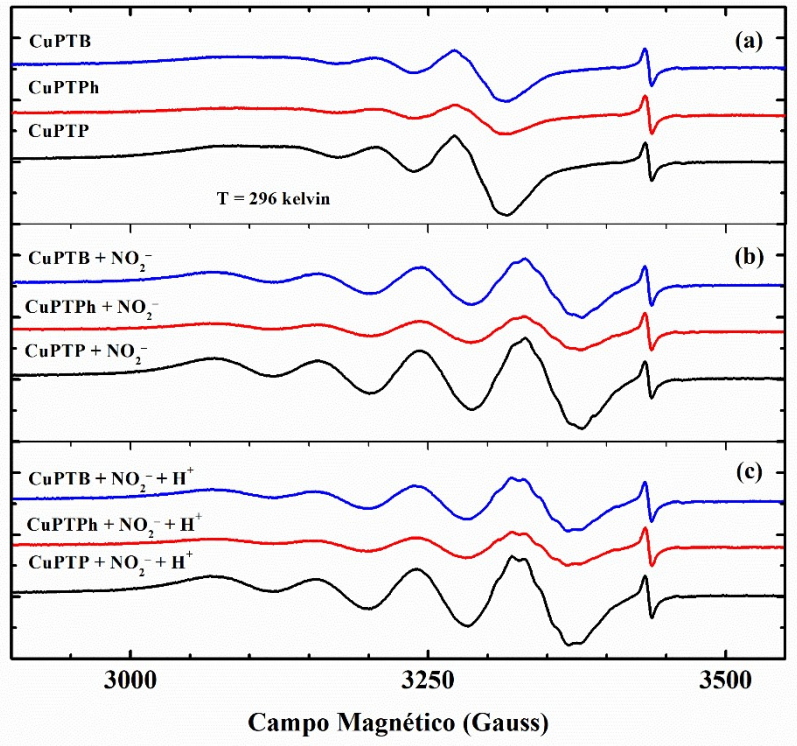

Fig. S 24 – EPR spectra of the copper complexes CuPTPh, CuPTB and CuPTP before (A) and after the addition of nitrite (B) and benzoic acid (C). All compounds were dissolved in methanol and the measurement was performed at room temperature (T = 296 kelvin). The signal in the high magnetic field is a Cr^{III} in MgO crystal used as a g-marker (g = 1.9797).

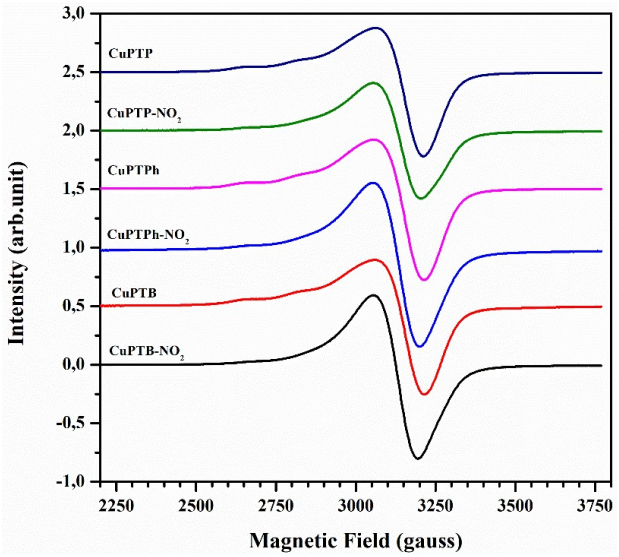

Fig. S25. EPR spectrum of solid state complexes in the absence and presence of nitrite.

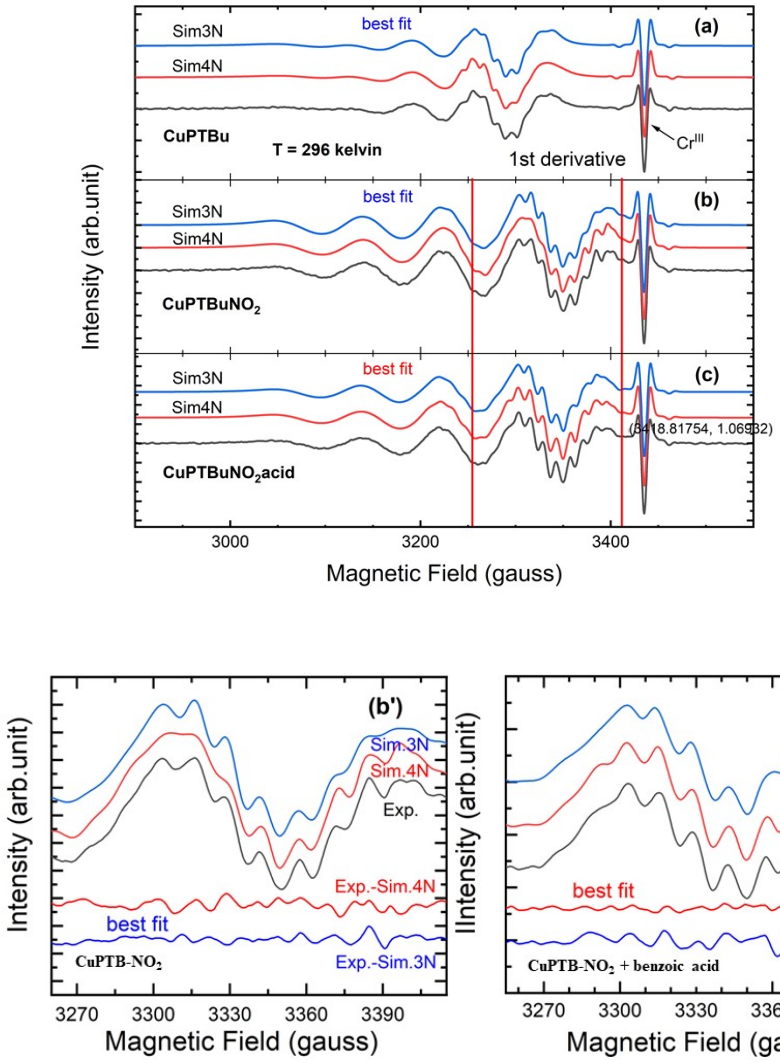

Fig. S26 – EPR spectra of the copper complex CuPTB in solution before (a) and after the

addition of nitrite (b) and benzoic acid (c). All compounds were dissolved in methanol and the measurement was performed at liquid nitrogen temperature (T = 77 kelvin). The signal in the high magnetic field is a Cr^{III} in MgO crystal used as a g-marker (g = 1.9797). Subtraction between simulation and experimental spectra for complex CuPTB-NO_2 in the presence and absence of acid are shown in (b′) and (c′), respectively.

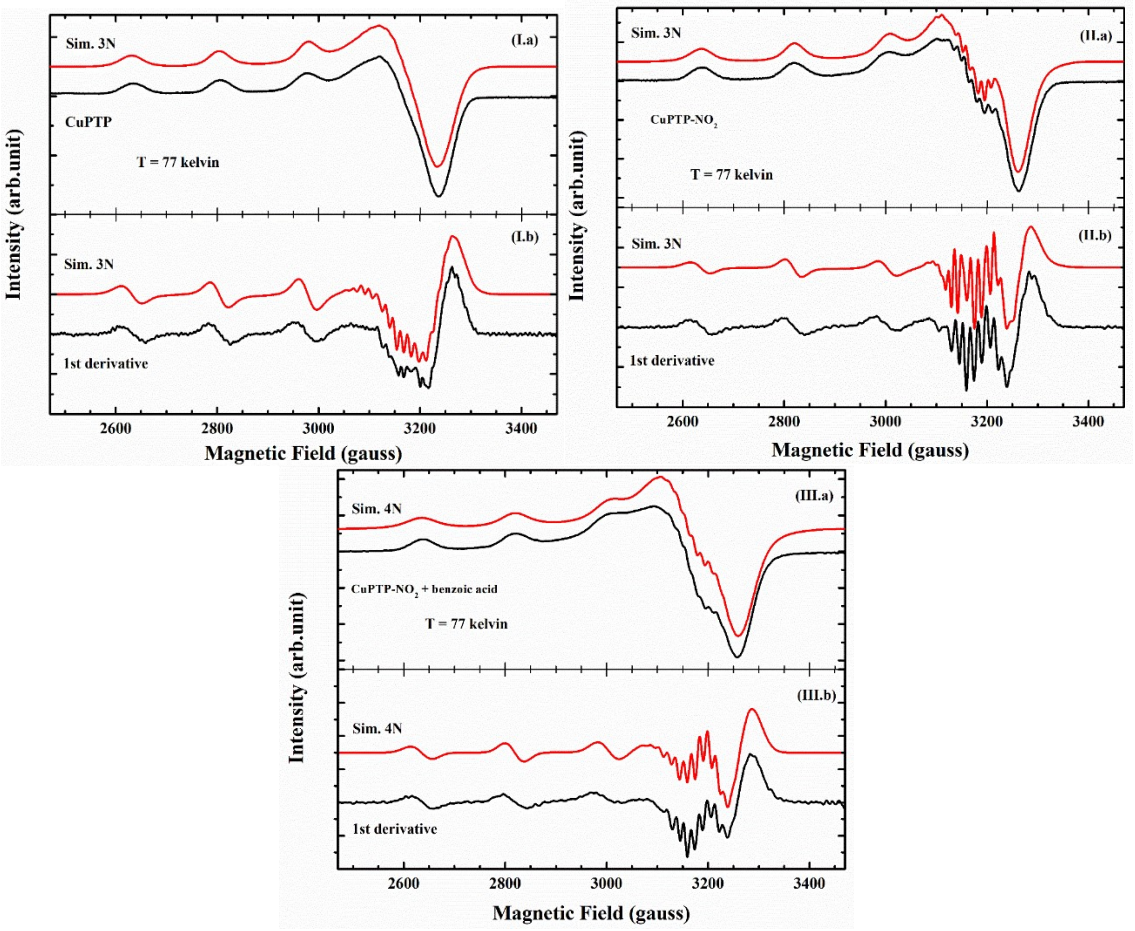

Fig. S27. EPR spectra and first derivative of (black) of the compounds CuPTP, CuPTP-NO_2 and CuPTP-NO_2 + benzoic acid in methanol solvent measured at liquid nitrogen temperature (T = 77 kelvin). Red spectral lines are simulations using 3 nitrogens ligands of Cu^{II} ions at compounds CuPTP and CuPTP-NO_2 and 4 nitrogens ligands of Cu^{II} ion at CuPTP-NO_2 + benzoic acid. The EPR parameters of the best fits are shown in Table S2. Simulations was done using Qpow program.

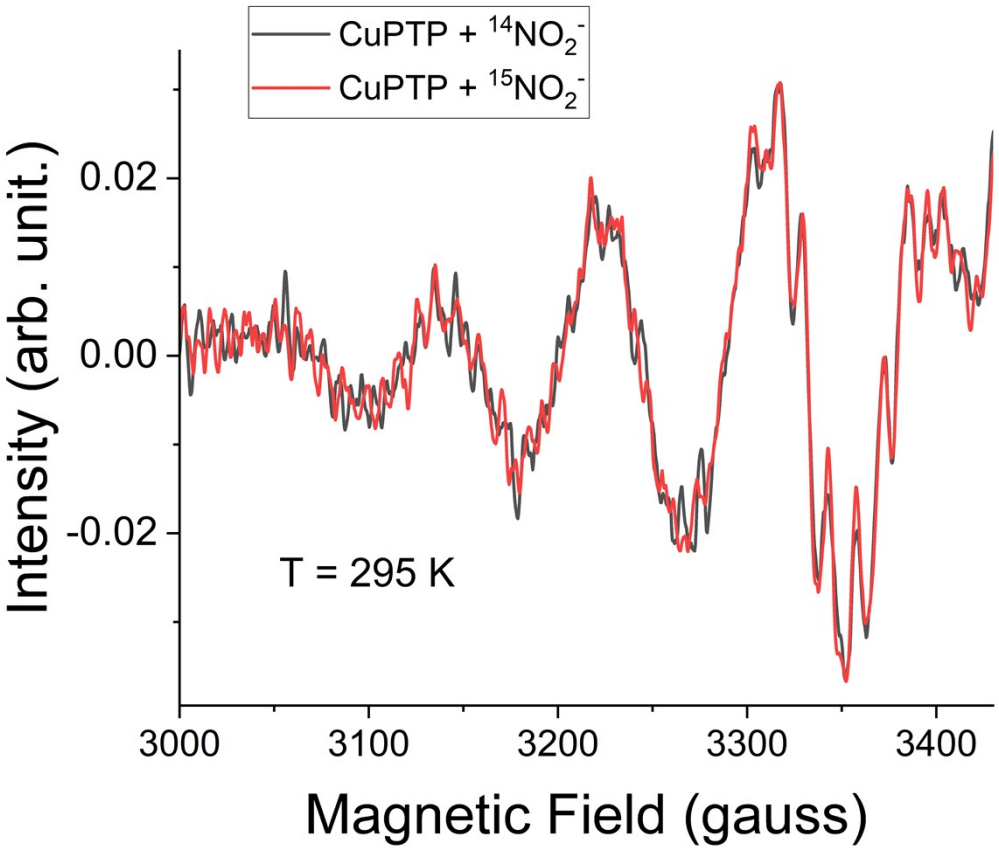

Fig. S28. EPR first derivative of CuPTP in the presence of $^{14}NO_2^-$ (black) and $^{15}NO_2^-$ (red) in methanol solvent measured at room temperature (T = 295 kelvin).

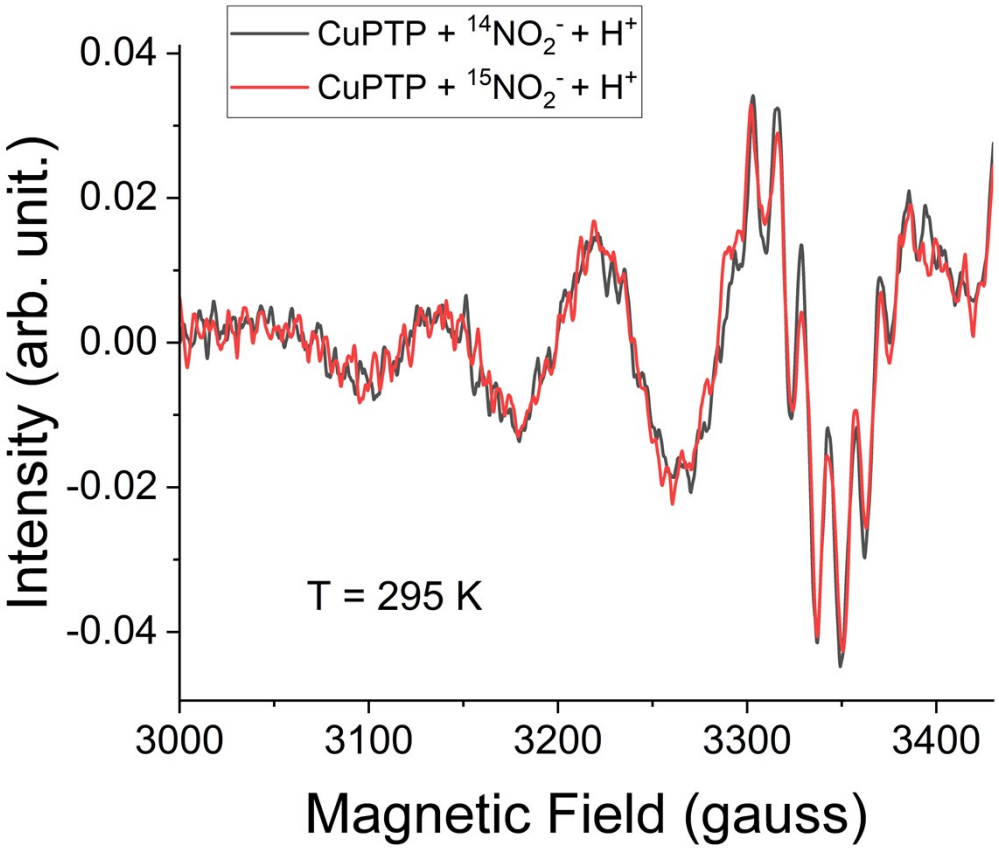

Fig. S29. EPR first derivative of CuPTP in the presence of 2 eq. benzoic acid and $^{14}NO_2^-$ (black) and $^{15}NO_2^-$ (red) in methanol solvent measured at room temperature (T = 295 kelvin).

Table S1: EPR Parameters for CuPTB, CuPTB-NO_2 and CuPTB-NO_2 + benzoic acid in MeOH solution at T = 296 Kelvin.

Compound	g_o	$A_{Cu}o$	$A_N{}^1o$	$A_N{}^2o$	$A_N{}^3o$	$A_N{}^4o$	Lw [G L]
CuPTB	2.1248	60.20	11.15	12.19	14.43	-	[3.99 1.10]
CuPTB-NO_2	2.1060	82.77	15.37	11.34	12,50	-	[3.99 1.10]
CuPTB-NO_2 + benzoic acid	2.1079	80.15	13.17	11.54	14.30	7.96	[3.39 0.92]

The values of $A_{Cu}o$, A_No and Lw are in gauss.

Table S2: EPR Parameters CuPTB, CuPTB-NO_2 and CuPTB-NO_2 + benzoic acid in MeOH solution at T = 77 Kelvin.

Compound	g [xyz]	A_{Cu} [x y z]	A_N [x y z]	Lw [x y z]	Q_{Cu} [u v]

CuPTB	2.0420 2.0780 2.2505	8.81 19.0 171.0	5.0 14.2 8.0	12.33 12.12 15.98	8.46 -3.88
CuPTB-NO_2	2.0550 2.0520 2.2340	21.7 21.8 181.9	10.5 14.4 6.5	8.75 8.81 16.10	8.40 -3.85
CuPTB-NO_2 + benzoic acid	2.0550 2.0520 2.2350	21.0 21.0 181.9	15.4 15.4 3.2	8.40 8.41 20.92	7.00 -3.50

The values of A_{Cu}, A_N, Q_{Cu} and Lw are in gauss.

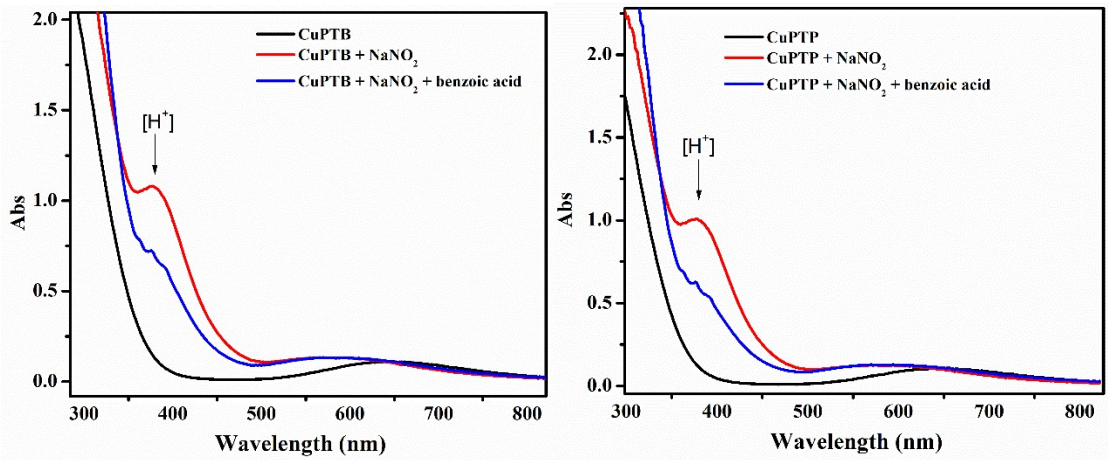

Fig. S30. Spectral change of complexes CuPTB and CuPTP after addition of 1 eq. of $NaNO_2$ and addition of 1 eq. of benzoic acid.

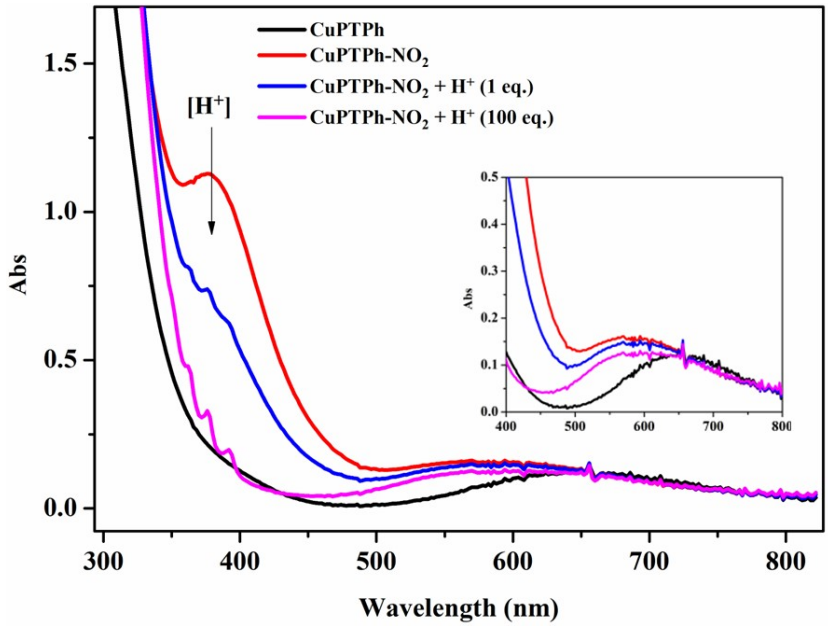

Fig. S31. Spectral change of complex CuPTPh after addition of 1 eq. of $NaNO_2$ and the addition of 1 eq. of benzoic acid or 100 eq. of benzoic acid. The inside graphic is an expansion of the 400-800 nm region of the spectra.

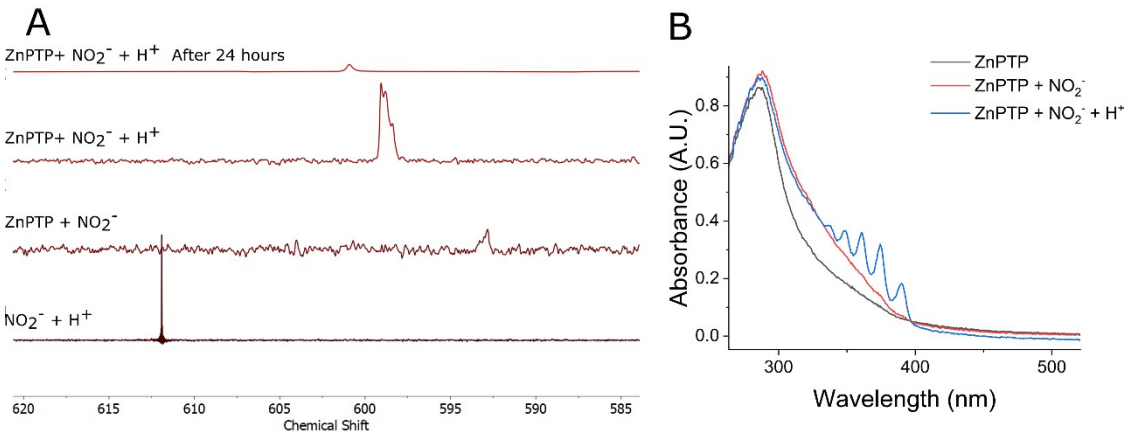

Figure S32. ^{15}N NMR spectra of ^{15}N nitrite in the presence of 2 eq of acetic acid, ZnPTP and ZnPTP and acid referenced to liquid NH_3. (A). UV-Vis spectral changes of ZnPTP upon addition of nitrite and its acidification (B).

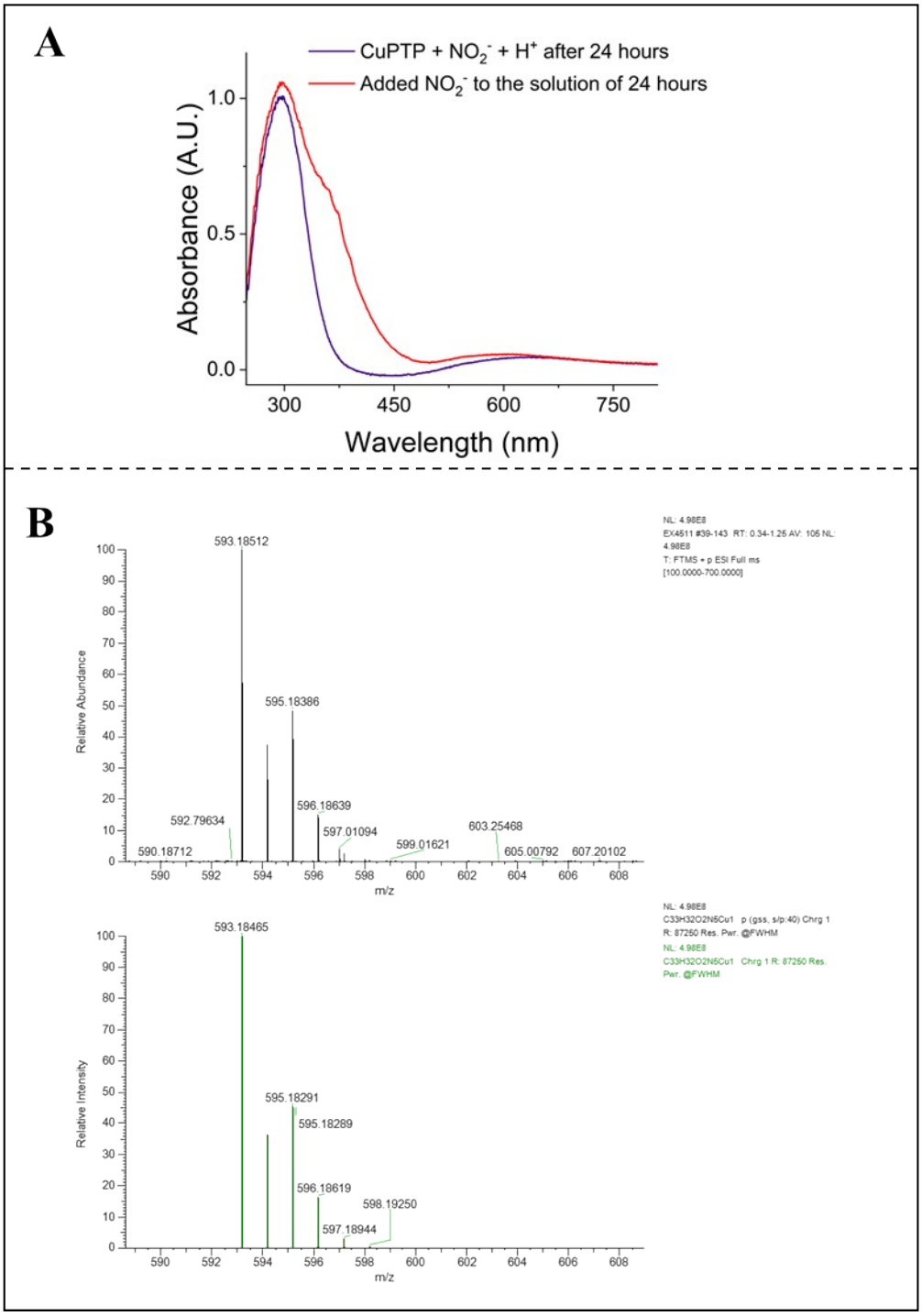

Figure S33. UV-Vis spectral changes of a solution of CuPTP with nitrite and acid after 24 hours before (blue line) and after the addition of more nitrite (red line) (A). HRMS of the solution of CuPTP with nitrite and acid after 24 hours (B).

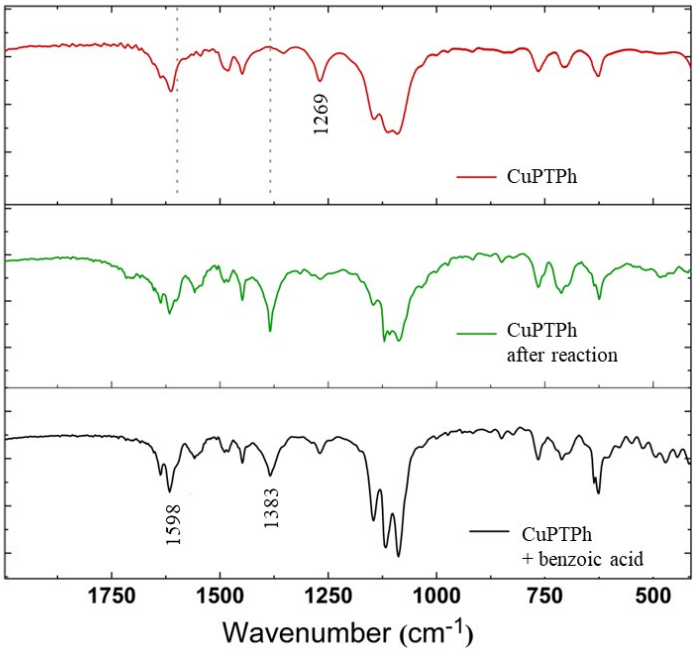

Fig. S34. FTIR Spectral change of complex CuPTPh (top), after the reaction with nitrite, benzoic acid and ascorbate (middle) and after incubation with benzoic acid (bottom).

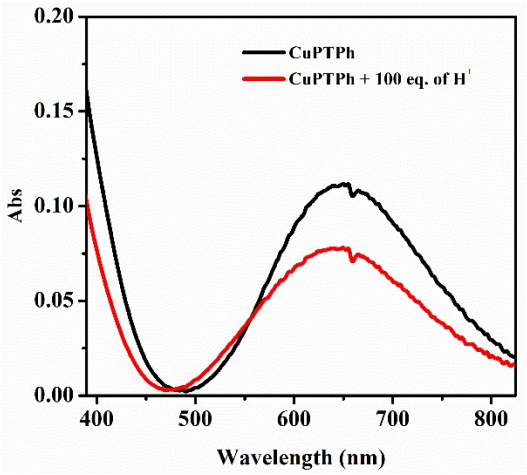

Fig. S35. Spectral change of complex CuPTPh after addition of 100 eq. of benzoic acid.

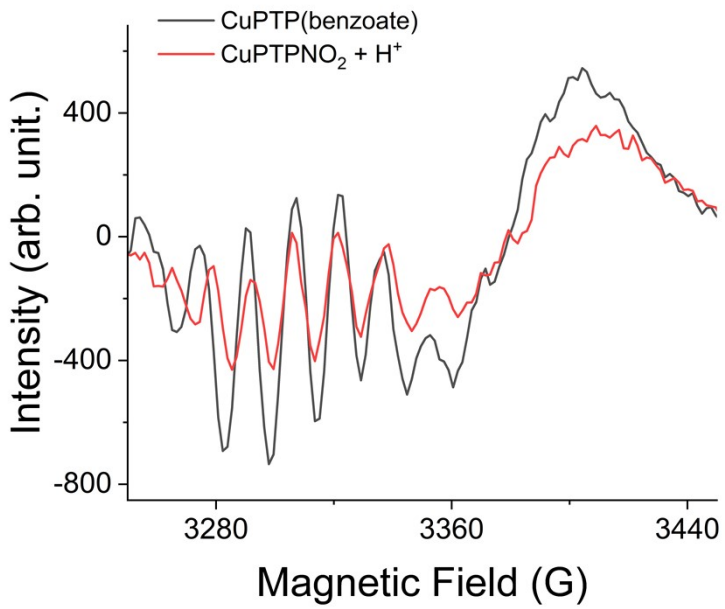

Fig. S36. EPR first derivative of CuPTP(benzoate) (black) and $CuPTPNO_2$ in the presence of benzoic acid (red) in methanol solvent measured at 123 kelvin.

6. Synthesis and characterization of ZnPTP

To 6 mL of methanol were added 58 mg of $Zn(ClO_4)_2.6H_2O$ (0.158 mmol) and 72 mg (0.158 mmol) of ligand PTP. The reaction proceeded at 50 °C for 4 hours. After that, the solvent was removed under reduced pressure. To remove any free ligand the yellow solid was washed with diethyl ether and dried (90% yield). Conductivity (μS cm^{-1}): 173,5 ± 0.4. FTIR in KBr (cm^{-1}): 3556, 3484, 3415; 2969, 2886; 1636, 1613; 1502, 1456; 1153 ,1126, 1094; 766, 712. Anal. Calcd for $C_{28}H_{35}Cl_2ZnN_5O_{11}$: C 42.57; H 4.98; N 8.87. Found: C 42.77; H 4.75; N 8.79.

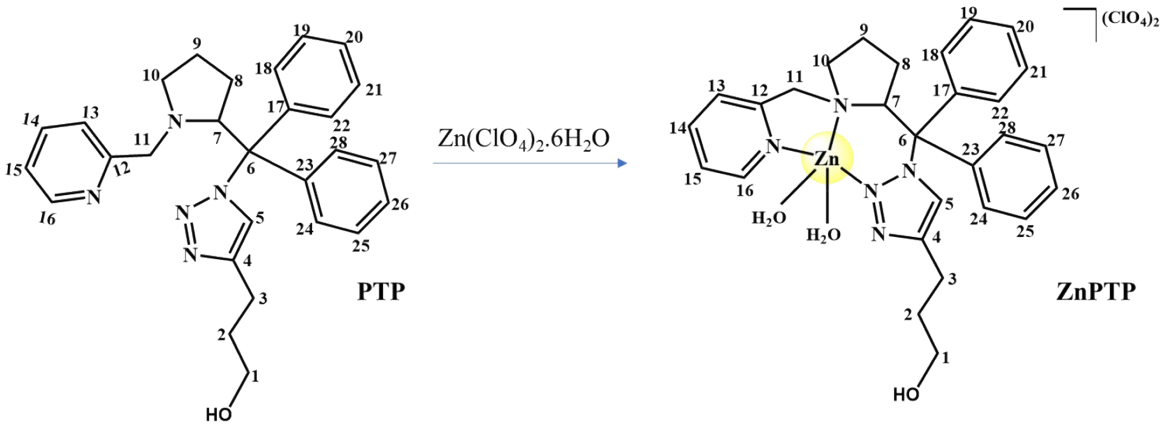

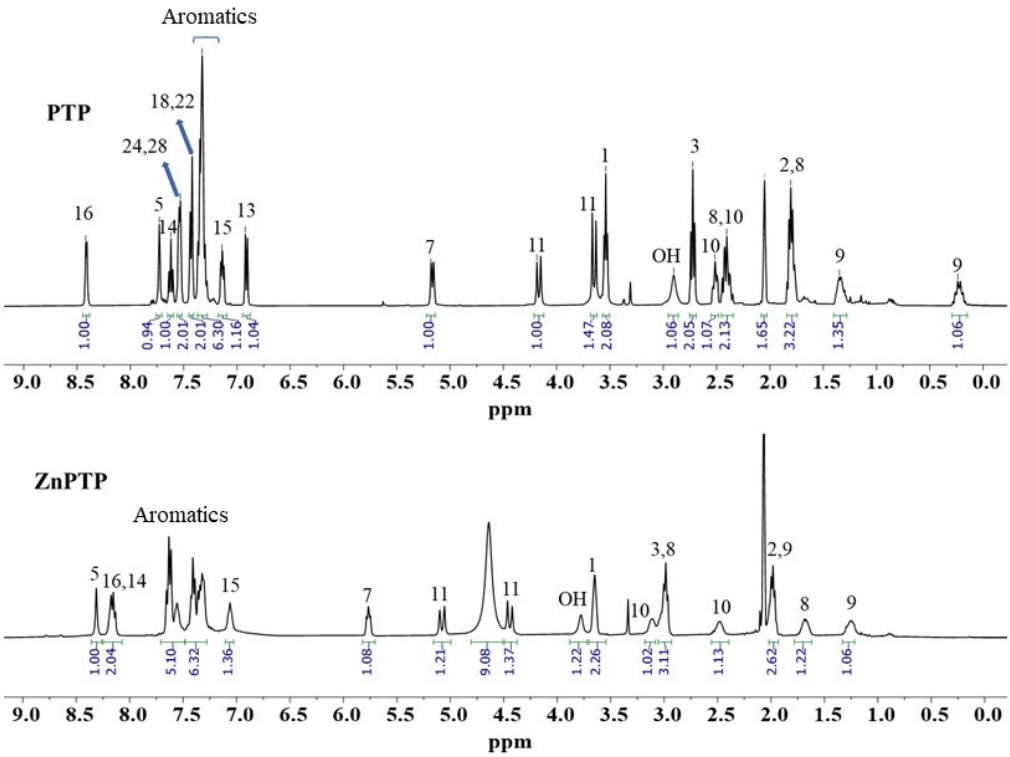

Fig. S37. [1]H NMR spectra of the ZnPTP complex and the free ligand.

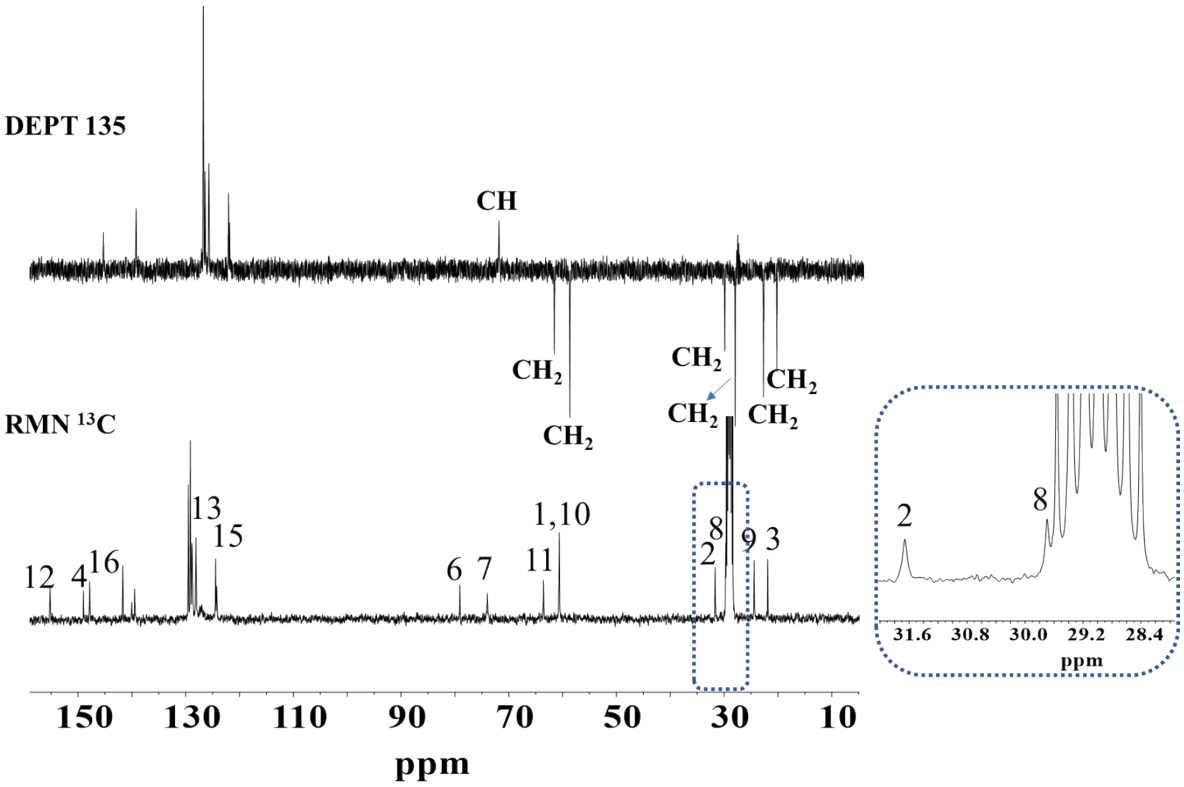

Fig. S38. [13]C NMR and DEPT 135 spectra of the ZnPTP complex.

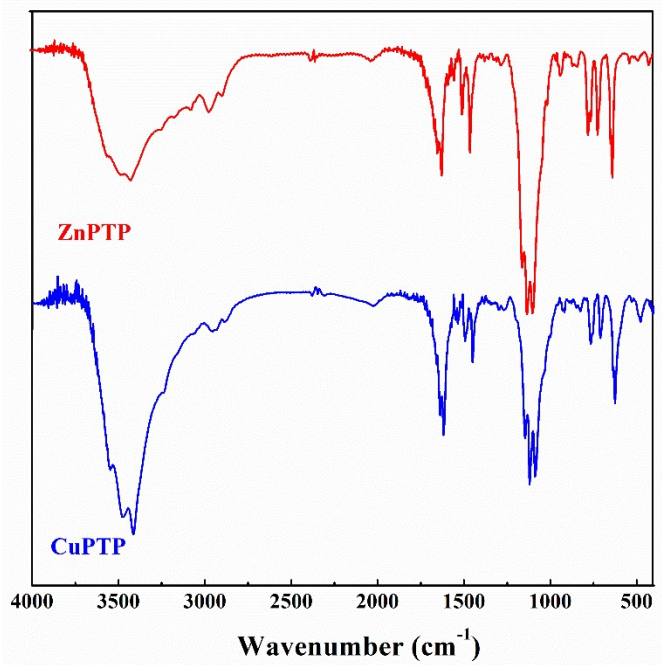

Fig. S39. FTIR spectrum of ZnPTP complex in KBr disk. Comparison with the CuPTP complex shows the similarity between the spectra.

7. Nitrite reduction

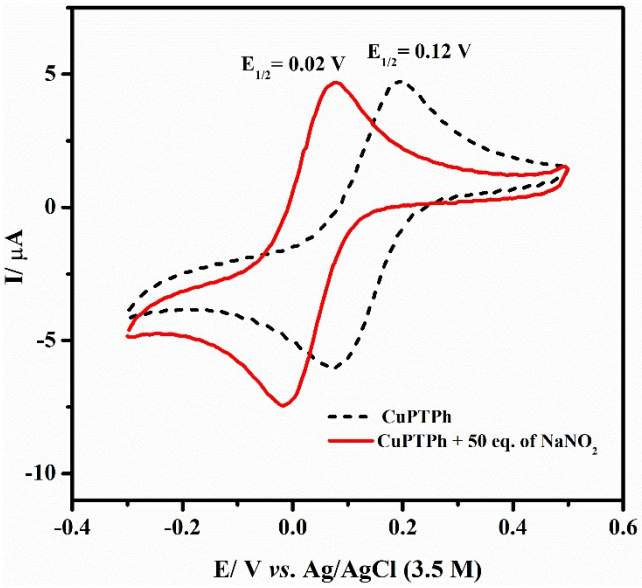

Fig. S40. Cyclic voltammogram of complex CuPTPh in the absence (black dots) and in the presence (red line) of 50 equivalents of sodium nitrite. The voltammogram was recorded in methanol solution using PTBA 0.1M as electrolyte and Ag/AgCl as reference.

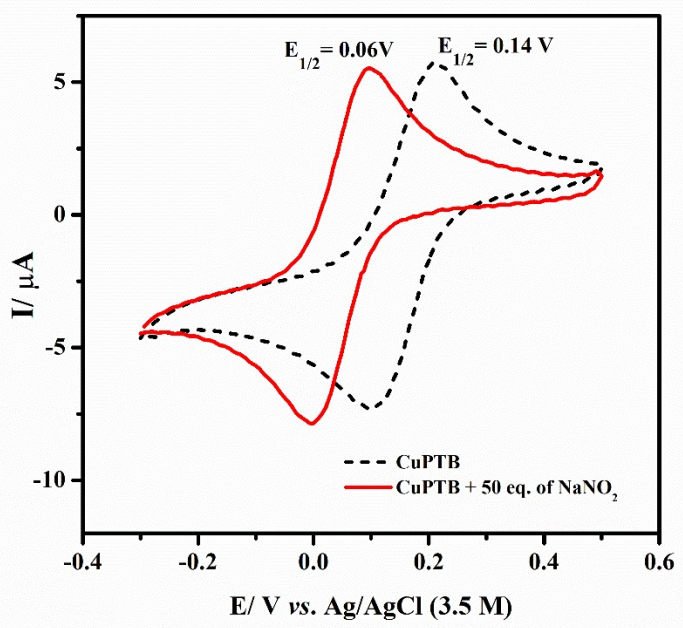

Fig. S41. Cyclic voltammogram of complex CuPTB in the absence (black dots) and in the presence (red line) of 50 equivalents of sodium nitrite. The voltammogram was recorded in methanol solution using PTBA 0.1M as electrolyte and Ag/AgCl as reference.

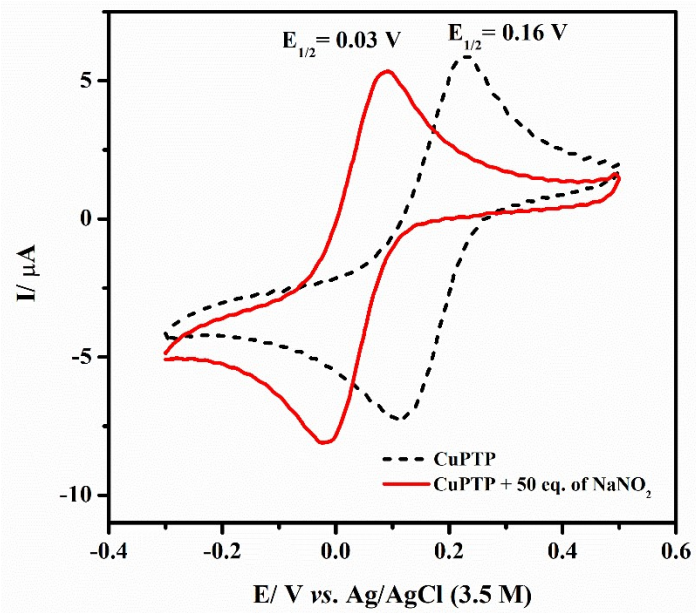

Fig. S42. Cyclic voltammogram of complex CuPTP in the absence (black dots) and in the presence (red line) of 50 equivalents of sodium nitrite. The voltammogram was recorded in methanol solution using PTBA 0.1M as electrolyte and Ag/AgCl as reference.

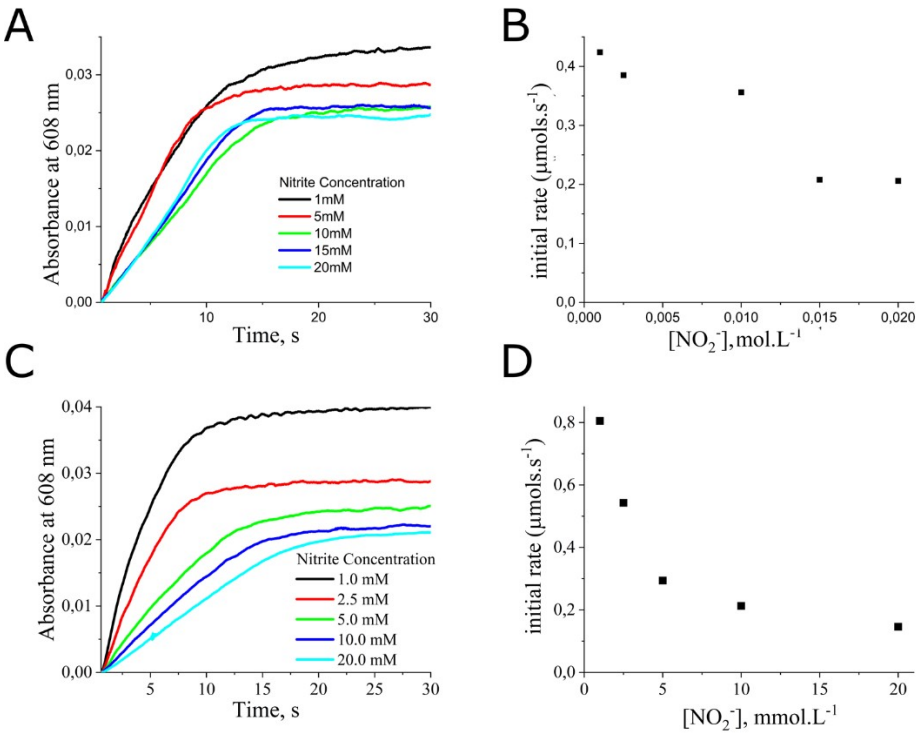

Fig. S43. Stopped-flow measurement of complexes CuPTPh and CuPTB following the 608 nm band with time at different nitrite concentrations (A and C) and the initial rate of nitrite reduction by complex CuPTPh and CuPTB upon nitrite concentration increase (B and D).

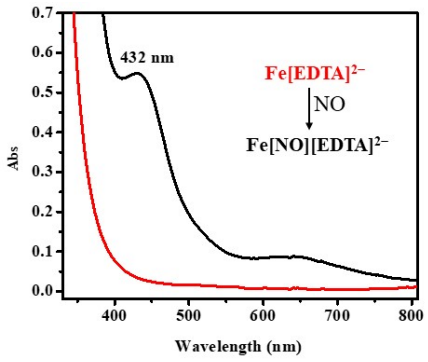

Fig. S44. UV-Vis spectrum of the [Fe(EDTA)]2- complex before and after coordination with NO.

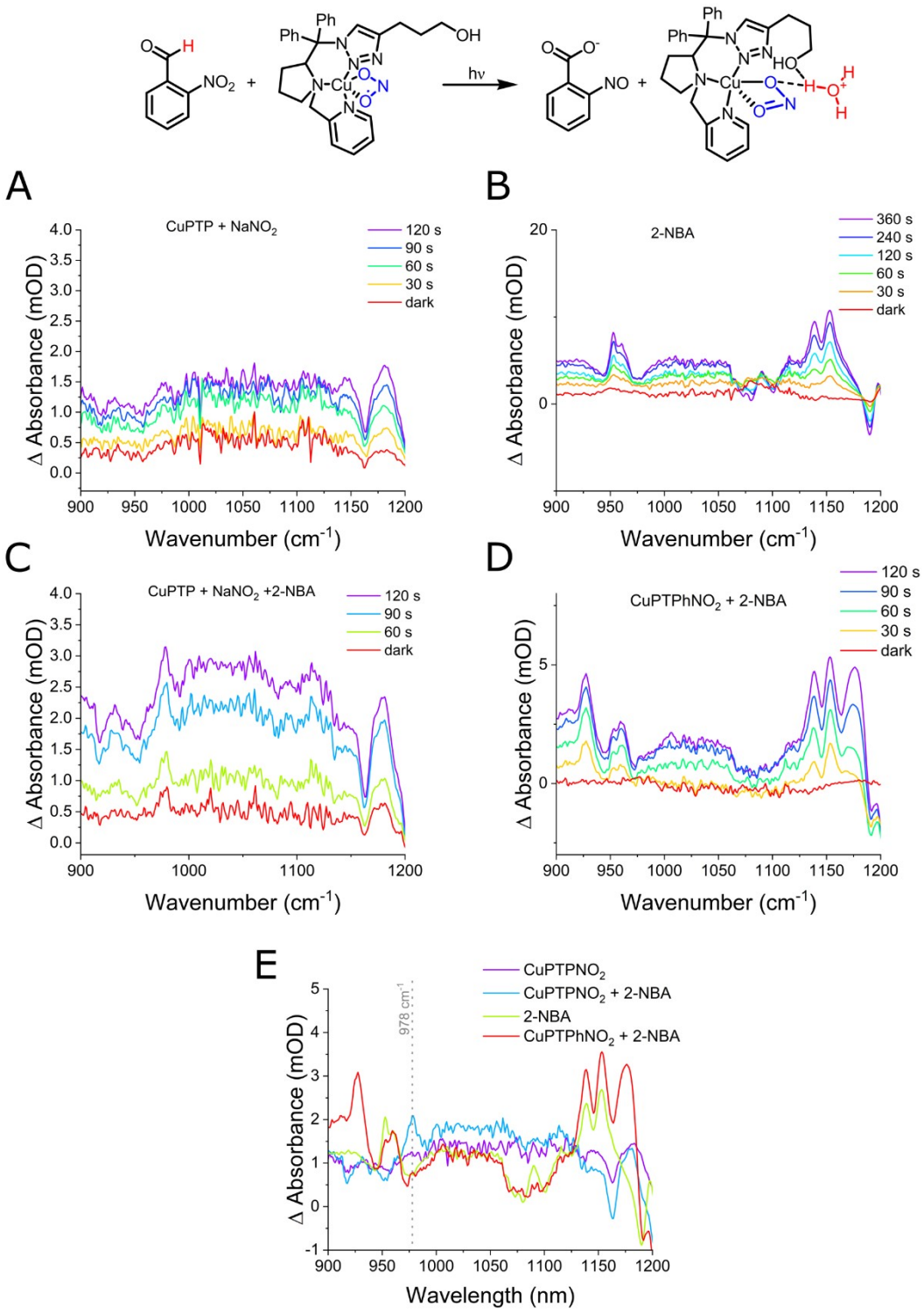

Fig. S45. Scheme of the photo titration of 2-NBA in the presence of CuPTPNO2 complex (A). Differential FTIR spectra of the photo titration of: 2-NBA in methanol (B) CuPTPNO2 in methanol (C) and CuPTPNO2 in the presence of 2-NBA in methanol (D). Comparison between the final spectrum of each photo titration (F). For the photo titration a diode laser λ=351 nm and power of 1KHz was used. The spectra are an accumulation of 1024 scans. The

dark spectra of B,C and D are from the subtraction of two subsequent spectra in the dark. The time indicated in the legend is the irradiation time of the sample.

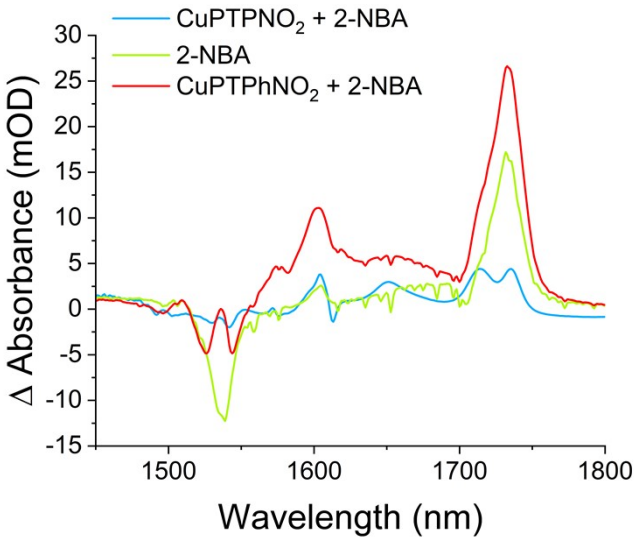

Fig. S46. Differential FTIR before and after photo titration of 2-NBA (green), CuPTPNO2 in the presence of 2-NBA (blue) and CuPTPhNO2 in the presence of 2-NBA (red).

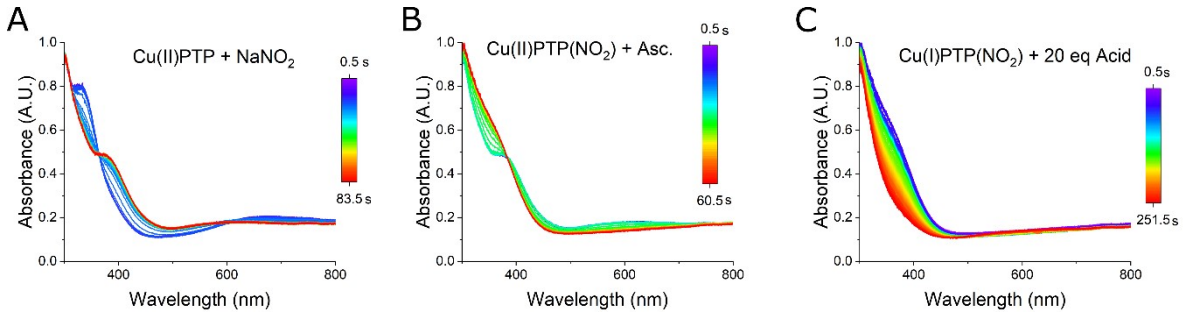

Fig. S47. UV-Vis spectra of CuPTP with stepwise addition of 1 eq. of nitrite (A), 3 eq. of sodium ascorbate (B) and 20 eq. of acetic acid (C).

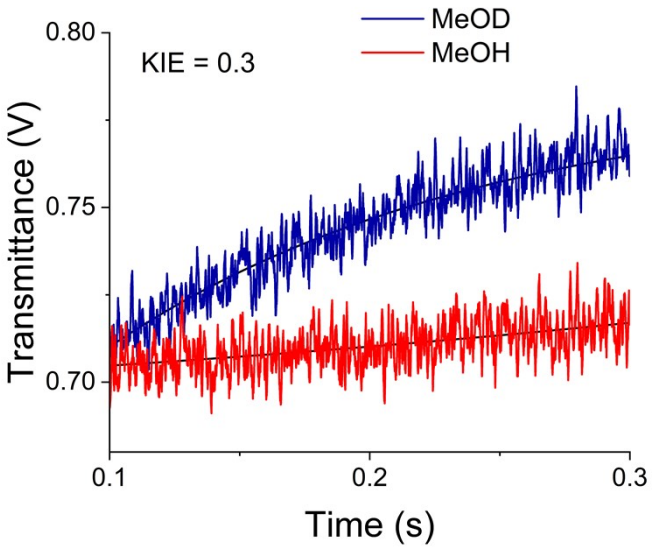

Fig. S48. Kinetic traces for the MLCT band at 395nm. Each trace represents the average of 7 consecutive shots and is fit to a single exponential grow. Measurement was performed by mixing a 5mM CuPTBNO$_2$ solution to 15mM of benzoic acid and 5mM of sodium ascorbate (Final concentrations 2.5mM CuPTB, 7.5mM benzoic acid and 2.5 mM of sodium ascorbate). 100% transmittance is 1.7V. A Xe-lamp coupled to a 365nm band pass filter was used as light. A 400nm short pass filter was added before the photomultiplier. For a better visualization of the difference data was smoothed with 27 points using Savitzky-Golay function on Origin 2022.

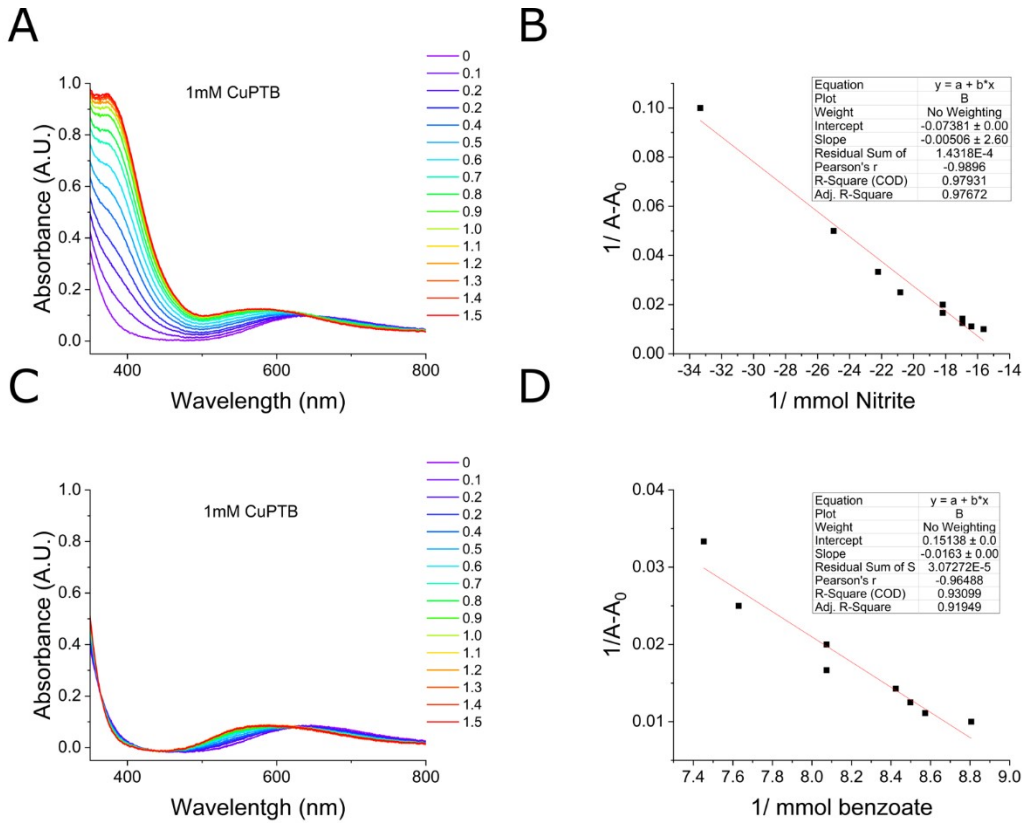

Fig. S49. Binding Constant of nitrite and benzoate determined by titration of a 1mL of 1mM CuPTB methanolic solution with aliquots of 1μL of 0.1M of the ligands. (A) titration with nitrite and (B) titration with benzoate. The slope of graphics of B and D is equal to $1/\Delta\varepsilon K[C]l$. Where Δε was determined at 580 nm by subtraction the ε_{580nm} at the start of the titration and after the titration in which [C] is the concentration of the complex and l is the optical path.

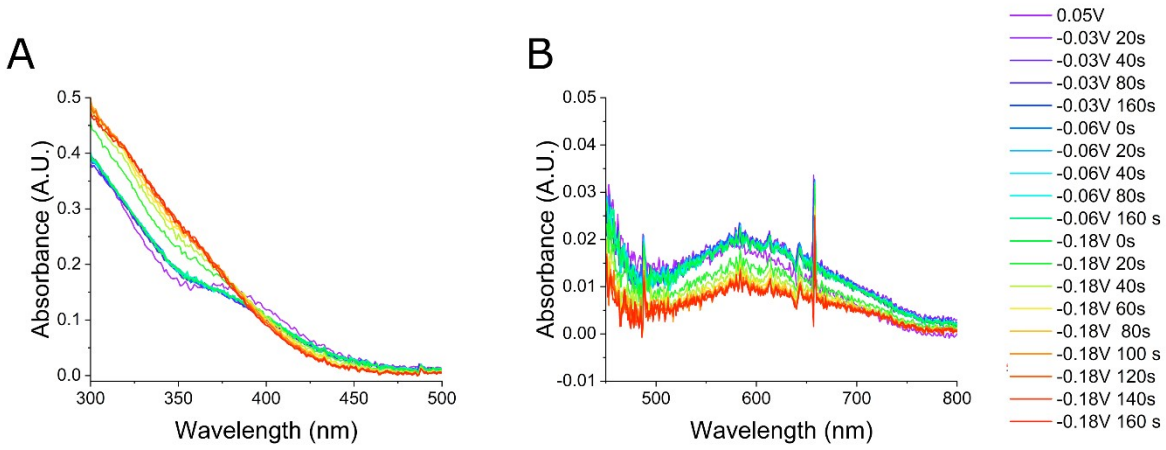

Fig. S50. Spectroelectrochemistry assay of a 0.5mM methanolic solution of $CuPTPNO_2$. (A) UV-Vis spectra between 300 and 500 nm evidencing the ligand to metal charge transfer band and (B) UV-Vis spectra between 450 and 800nm, evidencing the d-d band.

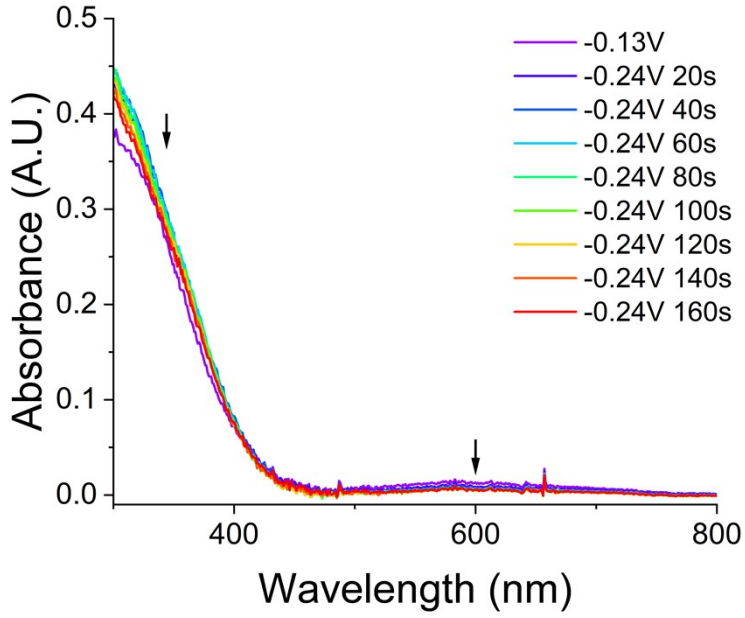

Fig. S51. Spectroelectrochemistry assay of a 0.5mM methanolic solution of $CuPTPNO_2$ in presence of 1mM benzoic acid applying potential of -0.24V (*vs* Ag/AgCl). The ligand to metal charge transfer band and the d-d band decreases with time, evidencing the conversion of nitrite into NO.

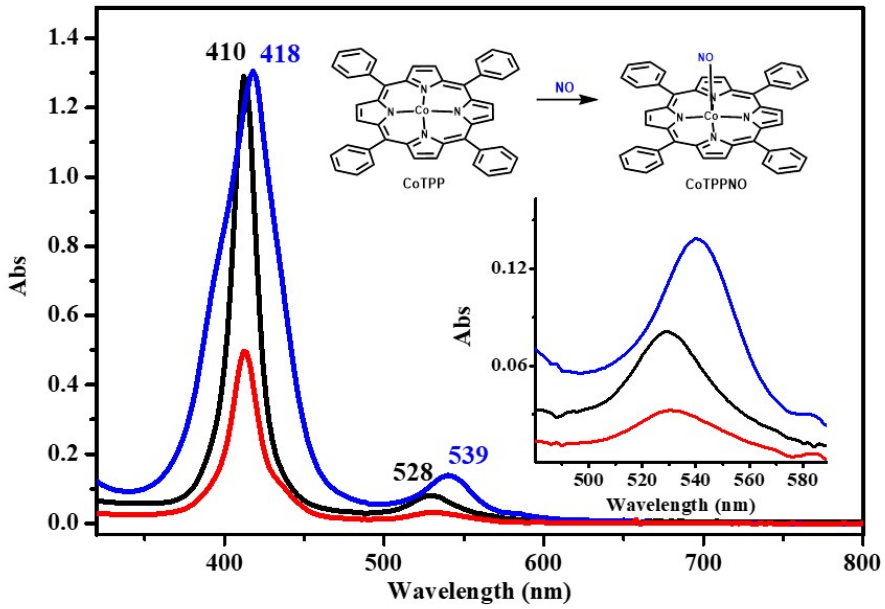

Fig. S52. UV-Vis spectrum of CoTPP porphyrin before (black line) and after (blue line) coordination with NO released in electrolysis. The spectrum of CoTPP performed from

electrolysis in the absence of copper complexes did not show band shifts (red line). Measurements were performed in CH_2Cl_2.

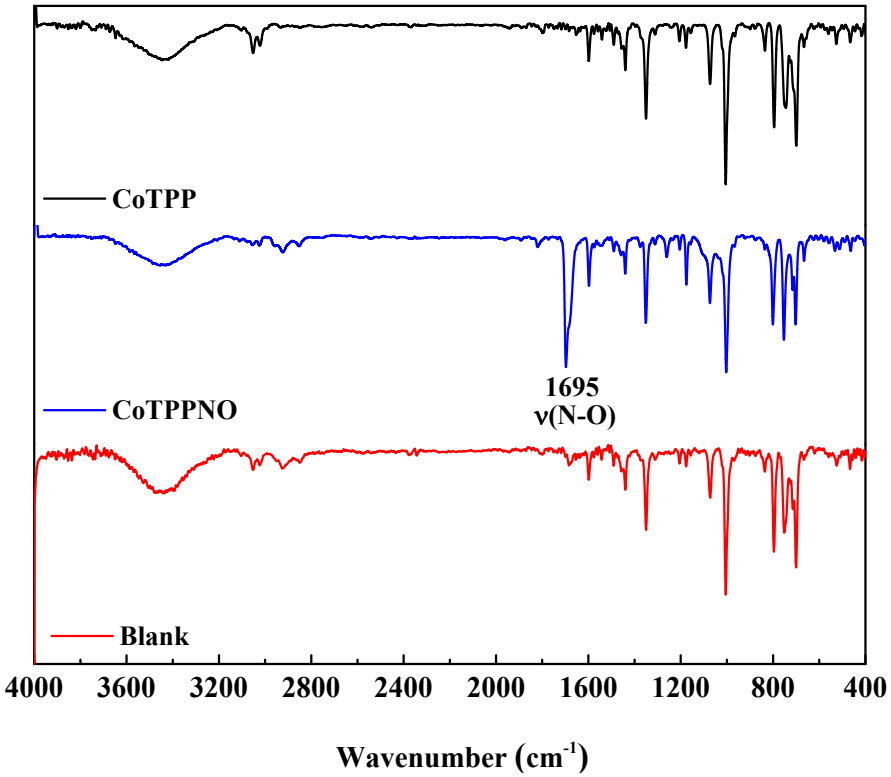

Fig. S53. IR spectrum of CoTPP porphyrin before (black line) and after (blue line) coordination with NO released in electrolysis. The spectrum of CoTPP performed from electrolysis in the absence of copper complexes did not show the appearance of ν(N-O) band (red line). Measurements were performed on KBr disk.

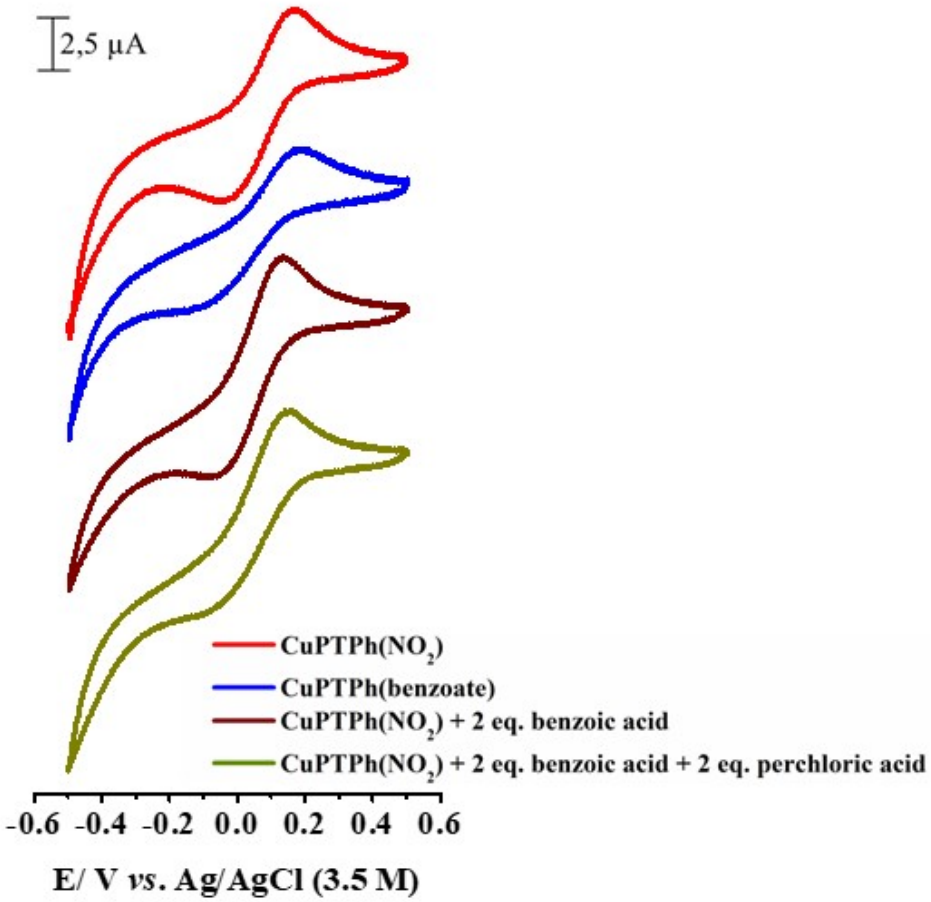

Fig. S54. Cyclic voltammogram of isolated CuPTPh, CuPTPh(benzoate) and CuPTP(NO_2). The cyclic voltammogram of complex CuPTP(NO_2) was also recorded in the presence of 2eq of benzoic acid and in the presence of 2eq of benzoic acid and 2eq od perchloric acid.

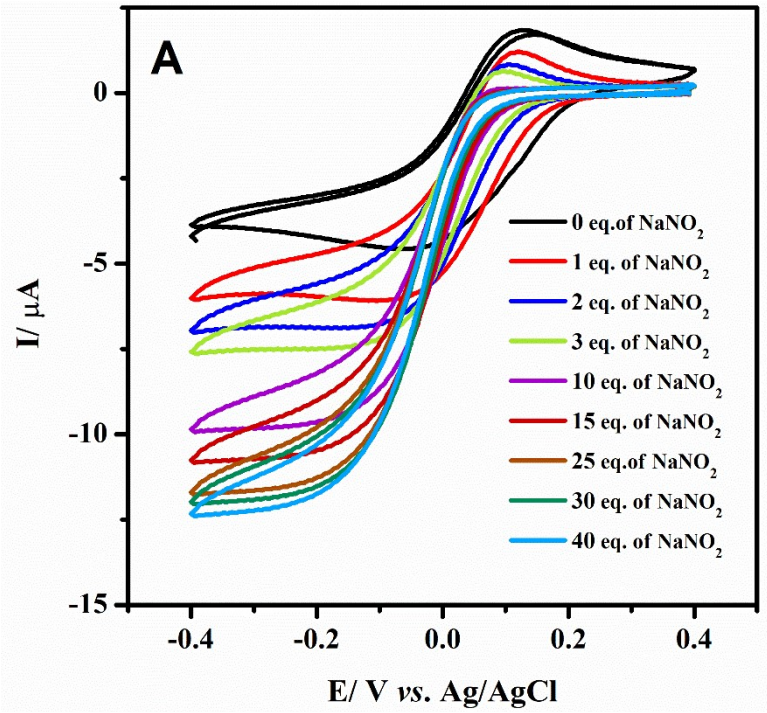

Fig. S55. Cyclic voltammogram of complex CuPTPh in the presence of 100 eq. de benzoic acid and increasing amounts of sodium nitrite.

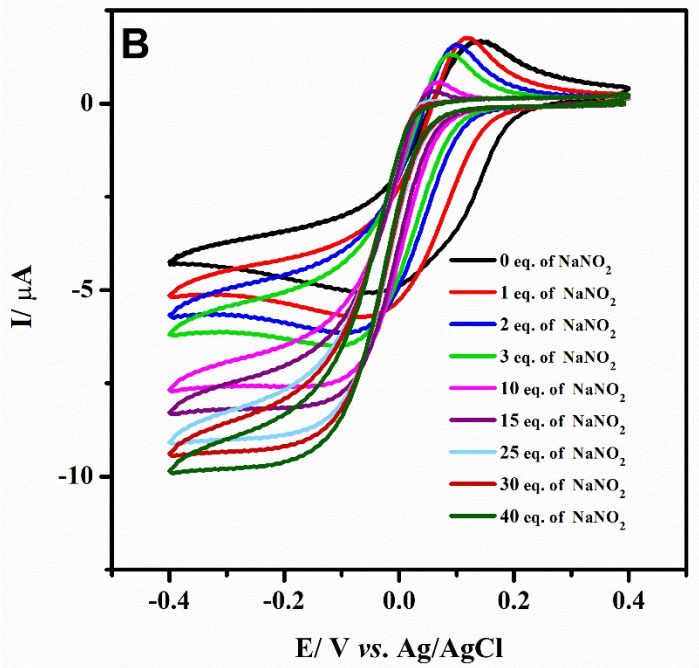

Fig. S56. Cyclic voltammogram of complex CuPTB in the presence of 100 eq. de benzoic acid and increasing amounts of sodium nitrite.

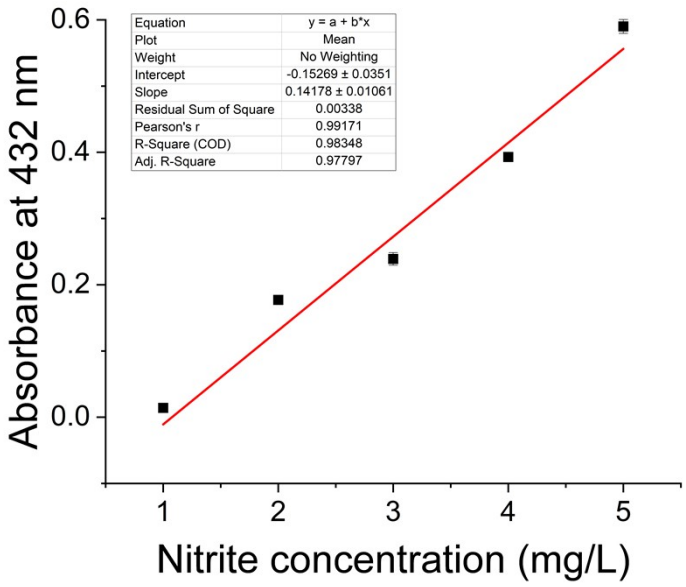

Fig. S57. Calibration curve of NO quantification. The absorbance at 432 nm relates to the formation of [Fe(EDTA)NO] complex.

8. **Crystallography for ligand PTB**

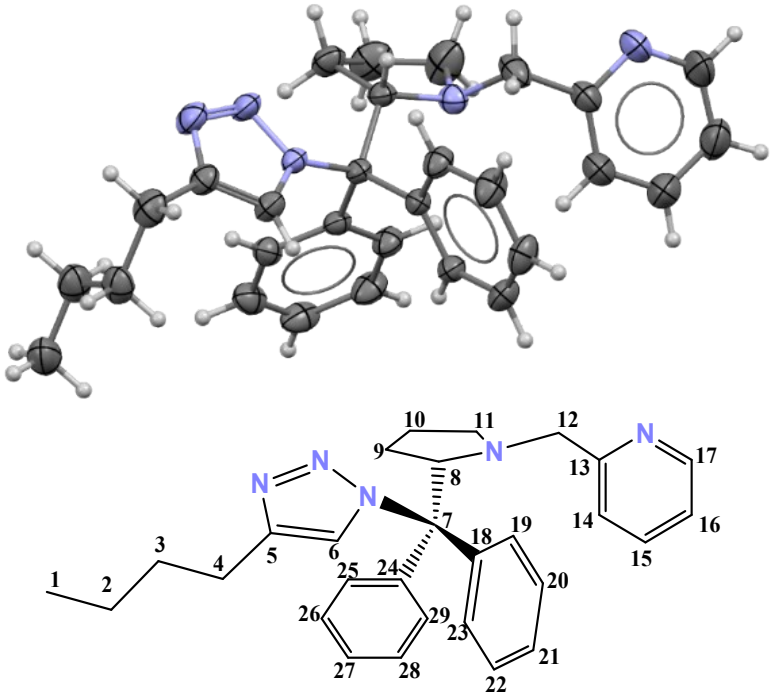

Figure S58. X-Ray structure and numbering assignments of ligand PTB.

Table S3 Crystal data and structure refinement for ligand PTB.

Identification code	2113820
Empirical formula	$C_{29}H_{33}N_5$
Formula weight	451.60
Temperature/K	293(2)
Crystal system	Monoclinic
Space group	P21
a/Å	9.8878(7)
b/Å	8.4324(7)
c/Å	15.4023(12)
α/°	90
β/°	98.845(7)
γ/°	90
Volume/Å^3	1268.94(17)
Z	2
ρ_{calc}g/cm^3	1.182
μ/mm^{-1}	0.071
F(000)	484.0
Crystal size/mm^3	0.427 × 0.291 × 0.24
Radiation	Mo Kα (λ = 0.71073)
2Θ range for data collection/°	5.29 to 52.74
Index ranges	$-12 \le h \le 12$, $-10 \le k \le 10$, $-19 \le l \le 19$
Reflections collected	26267
Independent reflections	5199 [R_{int} = 0.0296, R_{sigma} = 0.0209]
Data/restraints/parameters	5199/1/335

Goodness-of-fit on F^2	1.044
Final R indexes [I>=2σ (I)]	R1 = 0.0369, wR2 = 0.0935
Final R indexes [all data]	R1 = 0.0435, wR2 = 0.0996
Largest diff. peak/hole / e $Å^{-3}$	0.13/-0.13
Flack parameter	-0.3(6)

Table S4- Bond Lengths for ligand PTB.

Atom		Length/Å	Atom		Length/Å
N1	N2	1.309(3)	C9	C10A	1.517(9)
N1	C5	1.349(3)	C9	C10B	1.532(7)
N2	N3	1.334(2)	C10A	C11	1.394(10)
N3	C6	1.345(3)	C10B	C11	1.460(8)
N3	C7	1.488(2)	C12	C13	1.506(3)
N4	C8	1.485(3)	C13	C14	1.371(4)
N4	C11	1.460(4)	C14	C15	1.367(4)
N4	C12	1.441(3)	C15	C16	1.354(5)
N5	C13	1.322(3)	C16	C17	1.357(5)
N5	C17	1.335(4)	C18	C19	1.393(3)
C1	C2A	1.488(6)	C18	C23	1.380(3)
C1	C2B	1.590(12)	C19	C20	1.374(3)
C2A	C3A	1.485(6)	C20	C21	1.375(4)
C2B	C3B	1.546(16)	C21	C22	1.368(4)
C3A	C4	1.571(5)	C22	C23	1.382(3)
C3B	C4	1.457(13)	C24	C25	1.390(3)
C4	C5	1.495(4)	C24	C29	1.391(3)
C5	C6	1.356(3)	C25	C26	1.388(3)
C7	C8	1.569(3)	C26	C27	1.361(4)
C7	C18	1.540(3)	C27	C28	1.374(4)
C7	C24	1.533(3)	C28	C29	1.374(3)
C8	C9	1.543(3)			

Table S5- Angle Lengths for ligand PTB.

Atom			Angle/°	Atom			Angle/°
N2	N1	C5	109.50(18)	C10B	C9	C8	103.7(3)
N1	N2	N3	107.55(17)	C11	C10A	C9	106.7(6)
N2	N3	C6	109.48(17)	C11	C10B	C9	102.6(4)
N2	N3	C7	122.65(16)	C10A	C11	N4	108.5(4)
C6	N3	C7	127.23(16)	C10B	C11	N4	109.6(3)
C11	N4	C8	107.3(2)	N4	C12	C13	111.9(2)
C12	N4	C8	115.85(19)	N5	C13	C12	116.7(2)
C12	N4	C11	110.8(3)	N5	C13	C14	121.6(2)
C13	N5	C17	117.1(3)	C14	C13	C12	121.7(2)
C3A	C2A	C1	112.4(4)	C15	C14	C13	120.2(3)

C3B C2B C1	113.3(8)	C16 C15 C14	118.6(3)
C2A C3A C4	112.8(4)	C15 C16 C17	118.1(3)
C4 C3B C2B	109.4(8)	N5 C17 C16	124.4(3)
C3B C4 C5	111.3(5)	C19 C18 C7	118.95(16)
C5 C4 C3A	113.7(3)	C23 C18 C7	123.29(18)
N1 C5 C4	122.0(2)	C23 C18 C19	117.72(19)
N1 C5 C6	107.2(2)	C20 C19 C18	121.0(2)
C6 C5 C4	130.8(2)	C19 C20 C21	120.2(2)
N3 C6 C5	106.28(19)	C22 C21 C20	119.7(2)
N3 C7 C8	107.89(14)	C21 C22 C23	120.2(2)
N3 C7 C18	104.60(16)	C18 C23 C22	121.1(2)
N3 C7 C24	108.32(15)	C25 C24 C7	122.25(18)
C18 C7 C8	110.79(15)	C25 C24 C29	117.30(19)
C24 C7 C8	111.26(16)	C29 C24 C7	120.44(18)
C24 C7 C18	113.59(14)	C26 C25 C24	120.9(2)
N4 C8 C7	110.42(15)	C27 C26 C25	120.6(2)
N4 C8 C9	105.34(18)	C26 C27 C28	119.3(2)
C9 C8 C7	114.75(18)	C27 C28 C29	120.7(3)
C10A C9 C8	104.0(4)	C28 C29 C24	121.1(2)

9. Crystallography for complex CuPTPh

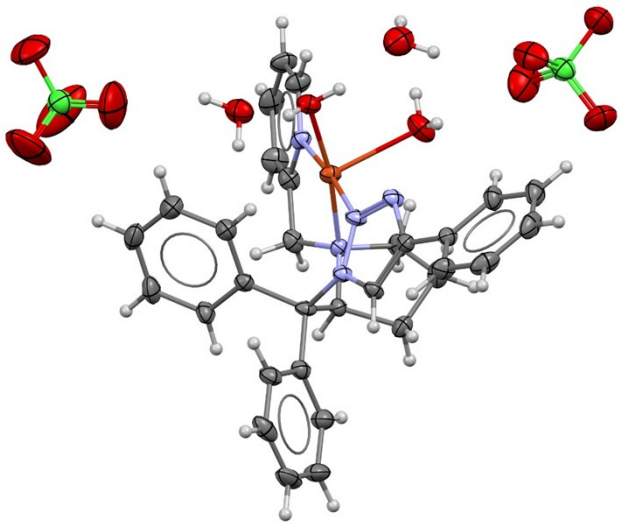

Table S6- Crystal data and structure refinement for complex CuPTPh.

Identification code	2113821
Empirical formula	$C_{31}H_{37}Cl_2CuN_5O_{12}$
Formula weight	806.09
Temperature/K	293(2)

Crystal system	tetragonal
Space group	$P4_3$
a/Å	9.0835(5)
b/Å	9.0835(5)
c/Å	42.651(4)
α/°	90
β/°	90
γ/°	90
Volume/Å³	3519.2(5)
Z	4
ρ_{calc}g/cm³	1.521
μ/mm⁻¹	0.842
F(000)	1668.0
Crystal size/mm³	0.182 × 0.137 × 0.117
Radiation	Mo Kα (λ = 0.71073)
2Θ range for data collection/°	4.874 to 51.348
Index ranges	$-11 \leq h \leq 9$, $-11 \leq k \leq 11$, $-45 \leq l \leq 52$
Reflections collected	17810
Independent reflections	5928 [R_{int} = 0.0414, R_{sigma} = 0.0491]
Data/restraints/parameters	5928/10/478
Goodness-of-fit on F^2	1.045
Final R indexes [I>=2σ (I)]	R1 = 0.0384, wR2 = 0.0838
Final R indexes [all data]	R1 = 0.0484, wR2 = 0.0887
Largest diff. peak/hole / e Å⁻³	0.33/-0.22
Flack parameter	-0.002(9)

Table S7- Main lengths and binding angles of the complex CuPTPh

Atom	**Length/Å**
Cu-O(1)	2.354(4)
Cu-O(2)	2.010(4)
Cu-N(2)	1.951(4)
Cu-N(4)	2.073(4)
Cu-N(5)	1.954(4)
	Angle/°
O(2)-Cu-O(1)	84.72(16)
N(2)-Cu-O(1)	93.12(16)
N(2)-Cu-O(2)	91.88(16)
N(4)-Cu-O(1)	103.27(16)
N(4)-Cu-O(2)	171.55(16)
N(5)-Cu-O(1)	91.87(17)
N(5)-Cu-O(2)	90.48(16)
N(5)-Cu-N(2)	172.65(17)
N(5)-Cu-N(4)	83.13(17)

10.DFT calculations results

The standard Gibbs free energy was computed for reaction depicted in equation (1). The relative stabilities of the HNO_2 conformations was evaluated and the *anti* conformation was the most stable for all ligands in the $[CuPTR\text{-}HNO_2]^{2+}$ complexes (Fig. 1), so this conformation was chosen for the remaining simulations.

$$[CuPTR\text{-}NO_2]^{+} + C_6H_5COOH \rightarrow [CuPTR\text{-}HNO_2]^{2+} + C_6H_5COO^{-} \quad \text{Equation (1)}$$

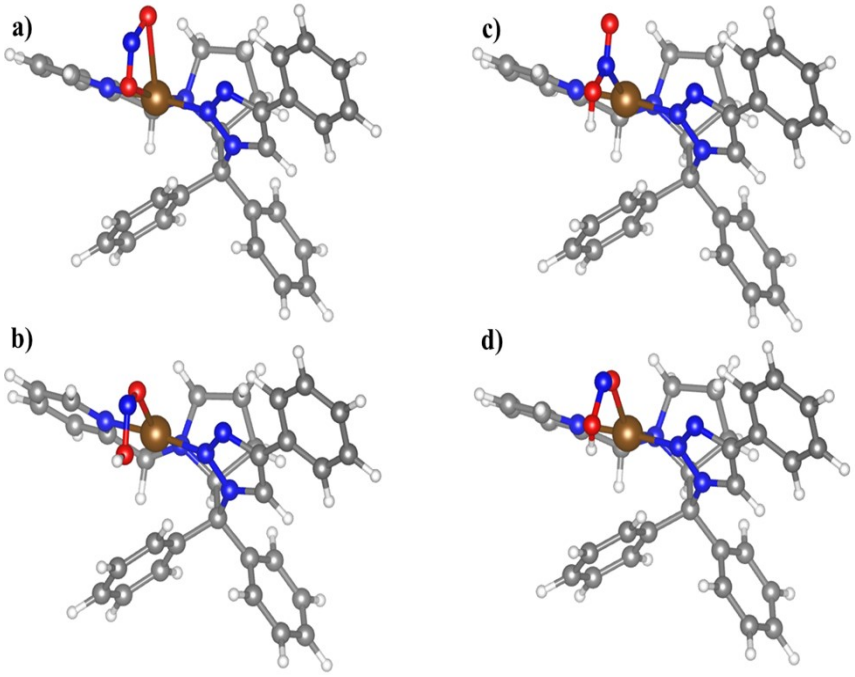

Fig. S59 – (a) CuPTPh-NO_2, (b) CuPTPh-*anti*-HNO_2, (c) CuPTPh-HNO_2 e (d) CuPTPh-*syn*-HNO_2.

The relative stability of the different ligands affected the Gibbs free energy for the proton transfer reaction (Table 1), but free energy differences should be analyzed with care since water molecules may fill up coordination positions and the free energy contributions arising from these extra molecules in the coordination shell of the complexes are larger than the differences arising from the sidechains themselves (Table 2). As might be expected, the larger hydration energy was observed for the system bearing a polar propanol side chain, as compared to the two hydrophobic chains. It is also noteworthy that adding a second water molecules yields a very small free energy contribution to the complex, smaller than the average thermal energy *3/2RT*, so the second water molecule should be regarded as a labile ligand. As a matter of fact, both water molecules should be seen as weakly bound to the complex since the Wiberg bond order computed for the Cu-O interaction was ca. 0.2, a value typically found for physical adsorption of molecules on solid surfaces, far below the values observed for the Cu-N interactions, which achieved bond orders twofold larger for all systems under investigation.

Table 1 – Gibbs Free energy computed for Equation (1) for the CuPT**R** systems with different sidechains (R).

R	**Gibbs free energy (kJ/mol)**
phenyl (Ph)	-153.2
n-butil (B)	-159.0
Propanol (P)	-154.1

$$[CuPT\mathbf{R}\text{-}(HNO_2)]^{2+} + nH_2O \rightarrow [CuPT\mathbf{R}\text{-}(HNO_2)\text{-}nH_2O]^{2+} \qquad \text{Equation (2)}$$

Table 2 – Calculated Gibbs Free energy for the CuPT**R**-HNO_2 systems.

CuPT**R**-(HNO_2)-n.H_2O	**Gibbs free energy (kJ/mol)**
Ph-Reference (Anhydrous)	0.0
Ph-H_2O^*	-10.3
Ph-$2H_2O$	-11.2
butil-Reference (Anhydrous)	0.0
butil-H_2O^*	-10.1
butil-$2H_2O$	-11.6
Propanol-Reference (Anhydrous)	0.0
Propanol-H_2O^*	-18.1
Propanol-H_2O	-20.4

***** Gibbs free energy average between H_2O position up or down bonding to Cu.

Besides being loosely bound, the second water molecules induced the formation of an extra band in the NIR region of the electronic spectrum (Fig. 2), which was not observed experimentally, so we should consider that one water molecule is the most probable hydration state of the complexes. The bands observed in the visible region arise from 8 transitions for the $[CuPTPh\text{-}HNO_2]^{2+}$ complex with one water molecule (position up), all of which have predominantly a LMCT character with some conribution of *d-d* transitions. In all transitions in the visible region the electron is excited to either LUMO (7 transitions) or LUMO+1 (1 transition), both of which have large contributions of *p* orbitals of the two oxygen atoms of the HNO_2 molecule (these orbital amount to *ca.* 38% in the case of the LUMO+1).

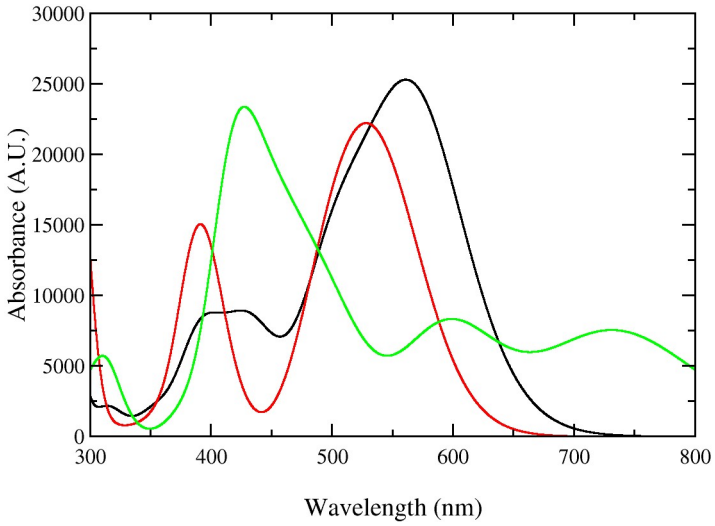

Fig. S60 - Calculated electronic absorption spectra for the $[CuPTPh\text{-}HNO_2]^{2+}$ complex with either one (red and black lines) or two water molecules (green line). The model systems with only one water molecule have distinct coordination positions of the water molecule, contributing to different UV-Vis spectra.

11. References

1. G. Cioncoloni, I. Roger, P. S. Wheatley, C. Wilson, R. E. Morris, S. Sproules and M. D. Symes, *ACS Catal*, 2018, **8**, 5070–5084.
2. P. Pracht, F. Bohle and S. Grimme, *Phys. Chem. Chem. Phys.*, 2020, **22**, 7169-7192.
3. S. Grimme, C. Bannwarth and P. Shushkov, *J. Chem. Theory Comput.*, 2017, **13**, 1989-2009.
4. C. Bannwarth, E. Caldeweyher, S. Ehlert, A. Hansen, P. Pracht, J. Seibert, S. Spicher and S. Grimme, *Wiley Interdiscip. Rev. Comput. Mol. Sci.*, 2020, **11**, e1493.
5. S. Ehlert, M. Stahn, S. Spicher and S. Grimme, *J. Chem. Theory Comput.* , 2021, **17**, 4250-4261.
6. W. Humphrey, A. Dalke and K. Schulten, *J. Mol. Graphics*, 1996, **14**, 33-38.
7. S. Grimme, *J. Chem. Phys.* , 2013, **138**, 244104.